Report

Cell Reports

Glia Modulate a Neuronal Circuit for Locomotion Suppression during Sleep in *C. elegans*

Graphical Abstract

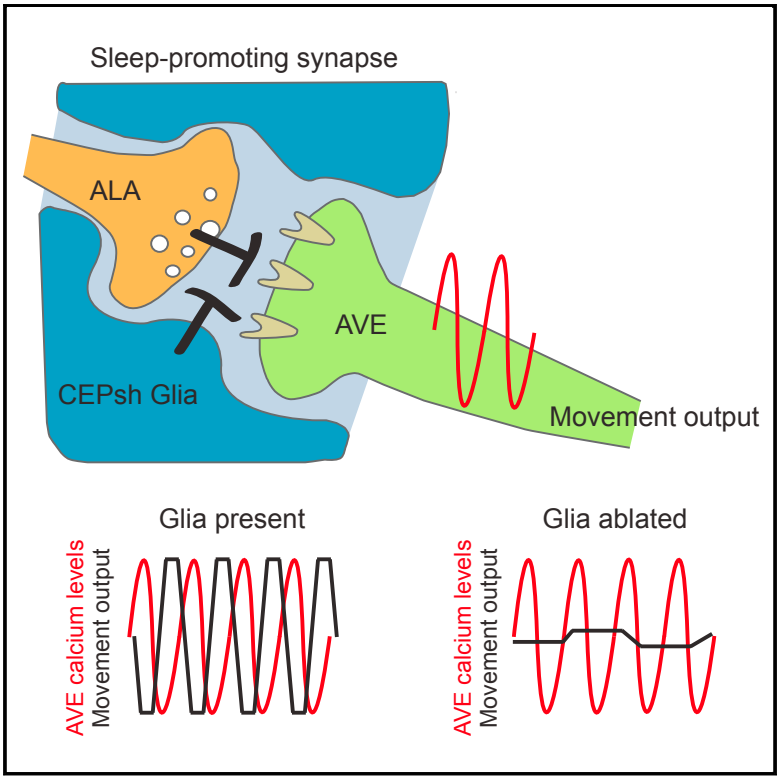

Authors

Menachem Katz, Francis Corson, Shachar Iwanir, David Biron, Shai Shaham

Correspondence

shaham@rockefeller.edu

In Brief

Sleep is characterized by reduced mobility. How neural circuits drive sleep-associated locomotion inhibition is not known. Here, Katz et al. demonstrate that neuron-associated glial cells prevent unintended sleep entry by inhibiting neuronal connections that promote sleep-related locomotion attenuation.

Highlights

- *C. elegans* CEPsh glia modulate locomotory quiescence during sleep
- Glia attenuate sleep-promoting inhibitory synapses between ALA and AVE neurons
- ALA promotes uncoupling of calcium transients and synaptic output in AVE

Katz et al., 2018, Cell Reports *22*, 2575–2583
March 6, 2018
https://doi.org/10.1016/j.celrep.2018.02.036

CellPress

Cell Reports
Report

Glia Modulate a Neuronal Circuit for Locomotion Suppression during Sleep in *C. elegans*

Menachem Katz,[1] Francis Corson,[2] Shachar Iwanir,[3,4] David Biron,[3] and Shai Shaham[1,5,*]
[1]Laboratory of Developmental Genetics, The Rockefeller University, 1230 York Avenue, New York, NY 10065, USA
[2]Laboratoire de Physique Statistique, Ecole Normale Supérieure, CNRS, Université Pierre et Marie Curie, Université Paris Diderot, 75005 Paris, France
[3]University of Chicago, GCIS E139F, 929 E. 57th St., Chicago, IL 60637, USA
[4]Present address: Department of Genetics, The Silberman Institute of Life Science, Edmond J. Safra Campus, Hebrew University of Jerusalem, Jerusalem 91904, Israel
[5]Lead Contact
*Correspondence: shaham@rockefeller.edu
https://doi.org/10.1016/j.celrep.2018.02.036

SUMMARY

Glia have been suggested to regulate sleep-like states in vertebrates and invertebrates alike. In the nematode *Caenorhabditis elegans*, sleep is associated with molting between larval stages. To understand if glia modulate neural circuits driving sleep in *C. elegans* larvae, we ablated the astrocyte-like CEPsh glia. We found that glia-ablated animals exhibit episodes of immobility preceding sleep, prolonged sleep, molting-independent short-duration locomotory pausing, and delayed development. CEPsh glia ensheath synapses between the sleep-associated ALA neuron and its postsynaptic partner AVE, a major locomotion interneuron. While AVE calcium transients normally correlate with head retraction, glia ablation results in prolonged calcium transients that are uncoupled from movement. Strikingly, all these glia ablation defects are suppressed by the ablation of ALA. Our results suggest that glia attenuate sleep-promoting inhibitory connections between ALA and AVE, uncovering specific roles for glia in sleep behavior. We propose that similar mechanisms may underlie glial roles in sleep in other animals.

INTRODUCTION

Sleep is an ancient and conserved behavior, whose purpose remains largely unknown (Zimmerman et al., 2008). Sleeping animals exhibit reduced motility, decreased responsiveness to the environment, and increased arousal thresholds (Brown et al., 2012), making them highly vulnerable to dangers such as predators. The benefits of sleep must, therefore, outweigh these considerable risks. Because sleep can be detrimental, the transitions in and out of this behavioral state must be prompt and tightly regulated. A number of mechanisms driving entry into and exit from sleep have been described. The circadian clock can influence sleep entry and recovery by regulating the activities of specific brain centers (Saper et al., 2005) or by controlling local brain circuits that collectively interact (Krueger et al., 2008). Homeostatic drivers such as adenosine, which accumulates during wakefulness, have also been suggested to play roles in sleep/wakefulness transitions (Brown et al., 2012).

In 1895, Ramón y Cajal postulated in a theoretical paper that astrocytic glia might be global modulators of sleep (García-Marín et al., 2007; Ramón y Cajal, 1895). A number of recent studies experimentally support this view. Astrocytes appear to be required for switching cortical activities between awake and sleep states (Poskanzer and Yuste, 2016). Consistent with this, optogenetic activation of astrocytes enhances the sleep state (Pelluru et al., 2016), and this may occur through the release of adenosine (Halassa et al., 2009) or by regulation of Notch signaling (Seugnet et al., 2011). Moreover, a number of studies implicate astrocytes in circadian behavior (Barca-Mayo et al., 2017; Brancaccio et al., 2017; Ng et al., 2011; Tso et al., 2017). Nonetheless, how sleep-promoting circuits are modulated by astrocytes to induce behavioral quiescence and whether this function is conserved is not clear.

A developmentally timed sleep-like state in the nematode *Caenorhabditis elegans* coincides with molting between larval stages (Raizen et al., 2008), and it is termed lethargus. Molting onset, duration, and associated sleep are regulated by LIN-42/Period protein (Jeon et al., 1999; Monsalve et al., 2011), whose homologs control circadian rhythms in insects and vertebrates. Like sleep in other animals, lethargus is characterized by behavioral quiescence, reduced sensory responsiveness, reversibility, homeostatic regulation, and stereotypical body posture (Cho and Sternberg, 2014; Iwanir et al., 2013; Nagy et al., 2014; Raizen et al., 2008; Schwarz et al., 2011). Several neurons have been implicated in *C. elegans* sleep and wakefulness, including the RMG, RIS, ALA, ASK, and RIA neurons, whose sleep-related activities involve responses to or release of specific neuropeptides (Choi et al., 2013; Nath et al., 2016; Nelson et al., 2013; Turek et al., 2013, 2016; Van Buskirk and Sternberg, 2007). Epidermal growth factor (EGF) and Notch signaling are also implicated in sleep control (Singh et al., 2011; Van Buskirk and Sternberg,

2007). Simultaneous imaging of nearly all *C. elegans* head neurons, using the calcium sensor GCaMP, reveals a reduction in activity of most neurons during lethargus (Nichols et al., 2017).

The *C. elegans* nerve ring is a brain-like neuropil consisting of most axons in the animal and harboring the majority of neuron-neuron synapses. This structure is associated with four CEPsh glial cells. These glia share a number of features with vertebrate astrocytes. Like astrocytes, CEPsh glia tile around the brain neuropil to define non-overlapping domains (Ogata and Kosaka, 2002; White et al., 1986). Within the neuropil, CEPsh glia ensheath a well-defined set of synapses (White et al., 1986), resembling vertebrate tripartite synapses that consist of neuronal synaptic pairs and astrocyte processes (Halassa et al., 2007). CEPsh glia also promote synaptogenesis (Colón-Ramos et al., 2007), an important function of vertebrate astrocytes (Eroglu and Barres, 2010). During development, CEPsh glia transform from simple bipolar cells to highly branched cells, reminiscent of the radial glia-to-astrocyte transition in vertebrates (Rapti et al., 2017). Importantly, CEPsh glia are enriched for gene transcripts also enriched in astrocytes, including the glial glutamate transporter *glt-1* (M.K., unpublished data) (Zhang et al., 2014). Glia-specific loss of GLT-1 in both *C. elegans* and vertebrates results in repetitive behaviors (M.K., unpublished data) (Aida et al., 2015).

Here, we show that CEPsh glia are important regulators of sleep entry in *C. elegans*. Ablation of these glia results in precocious sleep bouts during lethargus, increased sleep duration, and transient locomotory pausing in adults. Furthermore, larval development in glia-ablated animals is considerably prolonged. Remarkably, inactivation of the ALA neuron, whose synapses with the postsynaptic AVE interneuron are ensheathed by CEPsh glia processes, is sufficient to reverse all of these defects. Epistasis studies reveal that ALA, AVE, and CEPsh glia act in the same circuit, and activity imaging in AVE suggests that loss of CEPsh glia decouples input and output signals in this neuron, in a manner dependent on ALA. Our data highlight a specific synaptic connection mediating locomotion inhibition during sleep and suggest an integral role for glia in modulating this connection.

RESULTS

CEPsh Glia Regulate Sleep Entry, Adult Locomotory Pausing, and the Rate of Development

To determine whether *C. elegans* CEPsh glia play roles in sleep, we ablated all four cells in first-stage (L1) larvae, after nerve ring formation, using a reconstituted Caspase-3 gene expressed specifically in CEPsh glia (Chelur and Chalfie, 2007) (M.K., unpublished data), and we assessed the effects on locomotion during the L4-to-adult molt. As previously reported (Raizen et al., 2008), wild-type animals are constantly active during the intermolt period (Figures 1A, 1C, and S1A) and exhibit a single consolidated episode of elevated locomotion quiescence during the molt (Figures 1A, 1D, and S1A). However, the 3/3 CEPsh glia-ablated lines we generated experience ectopic quiescence bouts of ~20 min in duration, 1–2 hr before the beginning of a prolonged consolidated period of inactivity (Figures 1B, 1C, and S1A). As in both wild-type and glia-ablated animals consolidated quiescence of >2 hr is apparent, we define this period as lethargus. The shorter duration quiescence episodes preceding lethargus in glia-ablated animals are defined as precocious episodes. These observations demonstrate that CEPsh glia are required for regulating the transition between awake and sleep states. Consistent with these observations, we found that, in 2/3 glia-ablated lines, the main quiescence period is also prolonged (Figures 1D and S1A), suggesting that ablated animals exhibit a general propensity for sleep.

We wondered, therefore, whether CEPsh glia-ablated animals might also exhibit locomotory quiescence during adulthood, when animals no longer molt. To test this, we tracked the foraging behavior of adult animals on agar plates in the absence of food and used a Hidden Markov Model to identify states of motion and quiescence based on animal velocity (Experimental Procedures; Figures S1B–S1D). We found that, while wild-type animals exhibit continuous movement on plates, CEPsh glia-ablated adults display periods of locomotory pausing, which are variable between individual animals and which can last from a few seconds to several minutes (Figures 1E, S1D, and S1E; Movies S1 and S2). Of note, while reduced pharyngeal pumping normally accompanies lethargus-associated sleep in *C. elegans*, pumping rates are not altered in CEPsh glia-ablated adults (Figure S1F). Thus, glia appear to specifically control locomotory aspects of sleep, consistent with previous studies reporting that locomotion and pharyngeal pumping quiescence are regulated by different pathways (Nath et al., 2016).

To determine whether the ectopic pre-lethargus quiescence and the adult locomotory pausing seen in CEPsh glia-ablated animals are functionally related to lethargus quiescence, we examined animals defective in EGL-4, a cyclic GMP-dependent protein kinase expressed in many head neurons and previously characterized as a general regulator of sleep (Raizen et al., 2008). We examined animals carrying either a loss-of-function mutation (*ks62;* −) or a gain-of-function mutation (*ad450;* g) in the *egl-4* gene. We found that, in addition to reducing the quiescence fraction during lethargus (Figure S1G), loss of *egl-4*(−) also suppresses pre-lethargus quiescence and adult locomotory pausing in animals lacking CEPsh glia (Figures 1F and 1G). Consistent with these observations, gain of EGL-4 function increases quiescence during lethargus and adult locomotory pausing in glia-ablated animals (Figures 1G and S1G), although pre-lethargus quiescence was not affected in this mutant (Figure 1F).

Although the mechanism of EGL-4 function is not well understood, our genetic results using *egl-4* mutants nonetheless suggest that the various forms of locomotion quiescence we examined are likely related.

Finally, in addition to ectopic sleep bouts, we also observed a considerable developmental delay in CEPsh glia-ablated animals, a defect shared with *egl-4*(g) mutants (Figure S1H). While freshly laid wild-type embryos develop to adulthood within ~55 hr at 20°C, more than 20% of CEPsh glia-ablated animals only reach the L4 or younger larval stages after a similar amount of time (Figure 1H). This observation raises the possibility that increased somnolence slows development of the animal (see below).

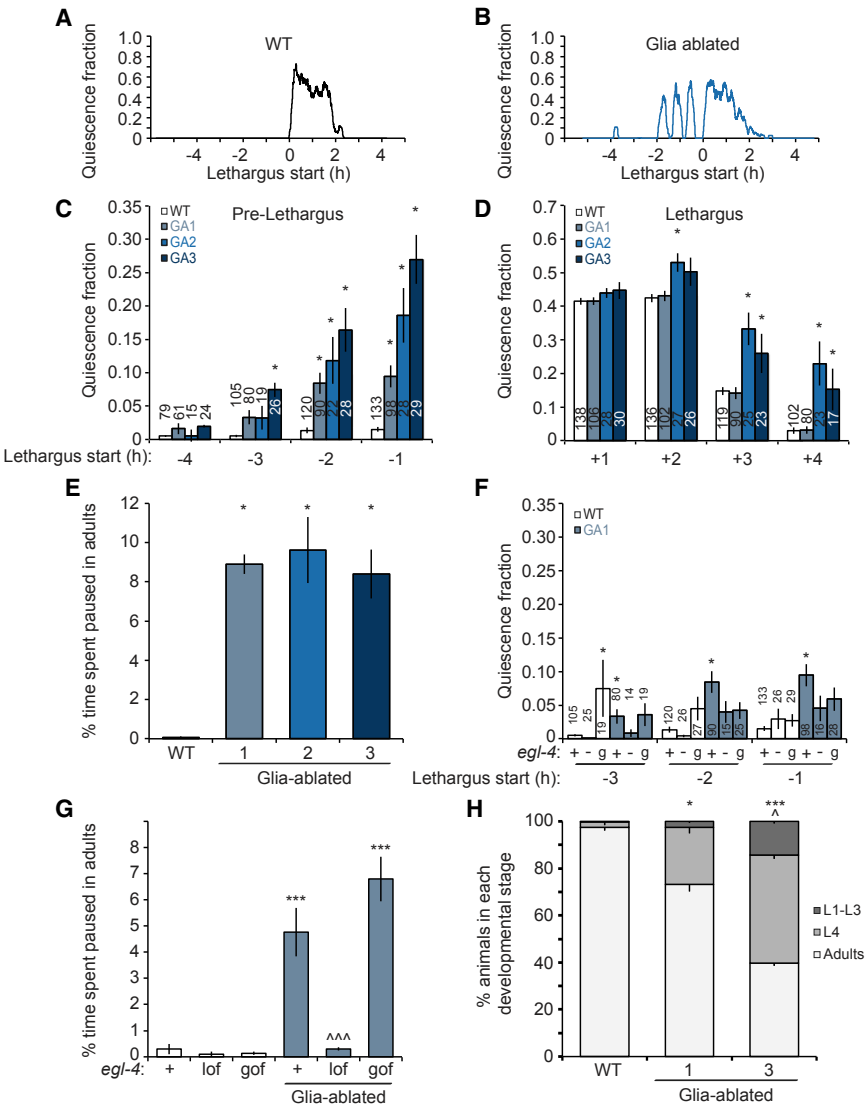

Figure 1. Post-embryonic Ablation of CEPsh Glia Affects Sleep Entry, Locomotion, and Development

(A and B) Traces of the quiescence fraction (Experimental Procedures) during the L4-adult transition of a wild-type (A) or a CEPsh glia-ablated (B) animal. Lethargus onset occurs at t = 0.

(C and D) Average quiescence fraction 4 hr before (C) and after (D) lethargus initiation, binned in 1-hr intervals. WT, wild-type. GA, glia ablated. Error bars indicate SE. Number of animals is indicated within or above each bar.

(E) Ablation of CEPsh glia results in enhanced pausing (n = 5 movies). Vertical axis represents the percentage of total time animals spent pausing out of the total duration of all recorded tracks.

(F and G) EGL-4 affects pre-lethargus quiescence (F) and ectopic adult pausing (G; n = 3 movies) of CEPsh glia-ablated animals (GA1). Loss-of-function mutation, −/lof; gain-of-function mutation, g/gof.

(H) Percentage of animals reaching a given developmental stage 55 hr after embryos are laid. Experiments were done in triplicate.

(C–H) Bar graphs, mean ± SEM; ANOVA Tukey's HSD post hoc test, *compared to WT, ^compared to glia-ablated line 1; number of symbols represents (1) $p < 0.05$ and (3) $p < 0.0005$.

See also Figure S1.

Taken together, our data suggest that CEPsh glia normally block locomotory quiescence and that their absence promotes ectopic quiescence during and outside the period of lethargus.

Ectopic Locomotory Quiescence and Developmental Delay Require the ALA Neuron

To understand how CEPsh glia block locomotory quiescence, we sought to identify neurons relevant to this glial function. In addition to ensheathing the nerve ring, CEPsh glia also send anterior processes that wrap around sensory endings of the dopaminergic CEP neurons. We found that ablation of CEP neurons in wild-type animals does not phenocopy CEPsh glia ablation and does not rescue ectopic locomotory pausing of CEPsh glia-ablated adults (Figure S1I). Thus, CEP neurons are unlikely to be the relevant targets of CEPsh glia in locomotion control.

Unlike most neurons, the ALA neuron remains active during sleep (Nichols et al., 2017), and its optogenetic activation suppresses motion (Fry et al., 2014; Nelson et al., 2014). Furthermore, ALA has been suggested to promote sleep entry (Van Buskirk and Sternberg, 2007). To test if locomotion quiescence observed in glia-ablated animals involves ALA, we disrupted the cell by either laser ablation or by crossing to a *ceh-17(np1)* mutant, which perturbs ALA development and activity (Pujol et al., 2000; Van Buskirk and Sternberg, 2007). While disruption of ALA has no effect on locomotion in wild-type adults, it significantly rescues the ectopic pausing episodes of CEPsh glia-ablated adults (Figures 2A and 2B). Importantly, loss of ALA function also fully rescues the pre-lethargus quiescence episodes (Figure 2C), the extended duration of lethargus (Figure S2A), and, remarkably, also the developmental delay (Figure 2D) of CEPsh glia-ablated animals. That *ceh-17* mutants alone do not exhibit defects in sleep control suggests that other parallel pathways likely also act to induce developmentally regulated sleep in *C. elegans*.

Together, these results suggest that all forms of ectopic quiescence episodes in CEPsh glia-ablated animals are a consequence of inappropriate activity of ALA. Thus, CEPsh glia may normally act to block ALA.

Activation of LET-23/EGF receptor (EGFR) in ALA controls sleep induced by heat and other stressors (Hill et al., 2014; Van Buskirk and Sternberg, 2007). To determine if glial effects on locomotion quiescence involve EGF signaling, we examined CEPsh glia-ablated animals also defective in *let-23(sy12)*. We found that these animals show enhanced pre-lethargus quiescence,

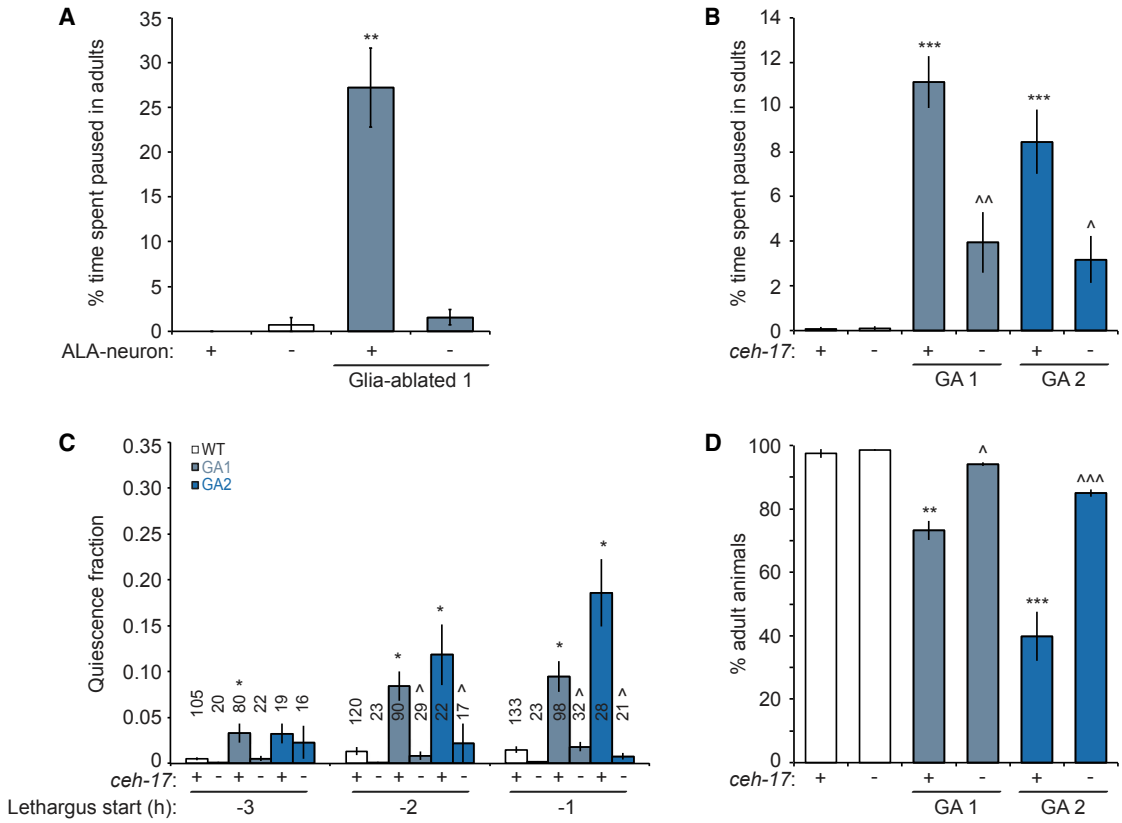

Figure 2. CEPsh Glia Ablation Defects Are Rescued by Disrupting ALA

(A) Ectopic pausing of CEPsh glia-ablated adults is suppressed by ALA ablation (−) (n = 2 movies). Details are as in Figure 1E.

(B) A *ceh-17* loss-of-function (−) mutation also suppresses ectopic pausing of CEPsh glia-ablated adults (n = 4 movies). Details are as in Figure 1E.

(C) A *ceh-17* mutation (−) suppresses ectopic pre-lethargus quiescence in CEPsh glia-ablated animals. Details are as in Figure 1G.

(D) A *ceh-17* mutation (−) restores normal development of CEPsh glia-ablated animals (experiments done in triplicate).

(A–D) Bar graphs, mean ± SEM; ANOVA Tukey's HSD post hoc test, *compared to WT, ^compared to glia-ablated parent; number of symbols represents (1) $p < 0.05$, (2) $p < 0.005$, and (3) $p < 0.0005$.

See also Figure S2.

prolonged lethargus duration, and increased locomotion pausing in adults, compared with CEPsh glia-ablated animals alone (Figures S2B–S2D). These observations suggest that LET-23 normally inhibits locomotory quiescence and that it can do so independently of CEPsh glia. Supporting this notion, ALA disruption does not significantly alleviate ectopic adult pausing of CEPsh glia-ablated animals also carrying a *let-23* mutation (Figure S2D). These results are consistent with previous reports suggesting that developmentally timed sleep and stress-induced sleep are regulated by different mechanisms (Trojanowski et al., 2015).

The AVE Neuron Functions Downstream of ALA and CEPsh Glia for Locomotory Quiescence

ALA has only five synaptic outputs, four of which target the backward locomotion command interneuron AVE, which synapses onto motor neurons (Chalfie et al., 1985; White et al., 1986). Three of the four ALA-AVE synapses are ensheathed by CEPsh glia processes, and they represent one of only two classes of such tripartite synapses known in *C. elegans* (White et al., 1986). These observations raise the possibility that AVE may be a relevant target for ALA during locomotion quiescence. To test this idea, we generated animals expressing tetanus toxin, which blocks synaptic neurotransmitter release, under the control of an AVE-specific promoter. These animals exhibit twitching movements primarily at the nose and tail tips (as opposed to locomotion) during lethargus, which prevented us from reliably assaying quiescence behavior during the sleep period (Figures S3A and S3B). However, we were able to follow ectopic locomotory pausing in adults. We found that, as with CEPsh glia ablation, AVE inhibition results in ectopic pausing (Figure 3A). By contrast, disruption of ALA does not rescue this pausing (Figure 3A). Importantly, ablation of both AVE and CEPsh glia does not enhance pausing beyond what is observed for CEPsh ablation alone (Figure 3B). Thus, AVE appears to function in the same circuit as and downstream of ALA and CEPsh glia in locomotion quiescence.

Since CEPsh glia ensheath ALA-AVE synapses, we wondered whether CEPsh loss may affect the structural integrity of these synapses. To test this, we generated animals expressing separate components of membrane-localized split-GFP (Feinberg

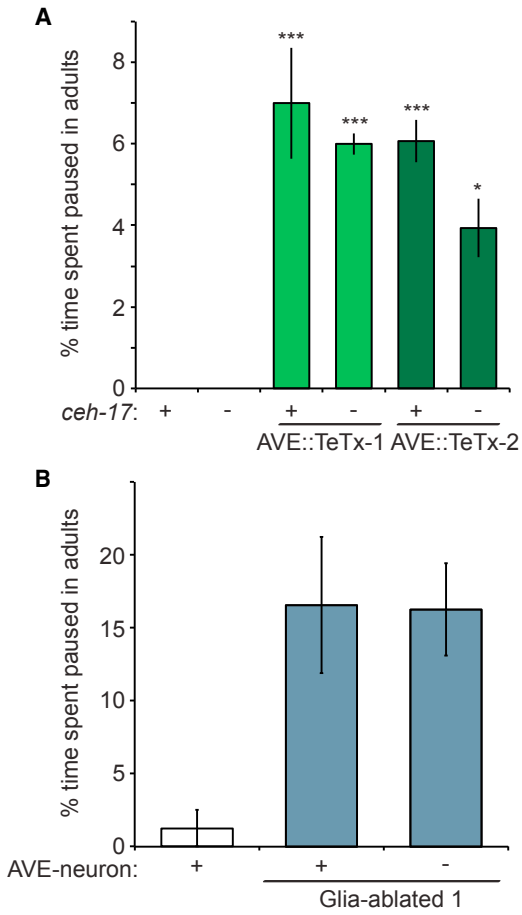

Figure 3. AVE Functions with ALA and CEPsh Glia to Control Locomotory Pausing

(A) Expression of tetanus toxin (TeTx) in AVE promotes ectopic pausing in adults, which is not rescued by a *ceh-17* mutation (−) (n = 3 movies). Details are as in Figure 1E.

(B) Ablation of AVE (−) does not enhance pausing of CEPsh-ablated worms (n = 2 movies). Details are as in Figure 1E.

(A and B) Bar graphs, mean ± SEM; (A) ANOVA Tukey's HSD post hoc test, *compared to WT; number of symbols represents (1) $p < 0.05$ and (3) $p < 0.0005$.

See also Figure S3.

et al., 2008) in ALA and AVE, using non-overlapping cell-specific promoters, and assessed membrane juxtaposition by GFP fluorescence. AVE postsynaptic sites were marked in these animals with mCherry-tagged neuroligin (Figure S3C). We found a comparable percentage of animals with intact synapses in wild-type and CEPsh glia-ablated animals (47% and 58%, respectively; n > 90). These results suggest that the effects of CEPsh glia removal are unlikely to be structural and may be a result of altered synaptic activity.

CEPsh Glia and ALA Control Coupling between AVE Calcium Elevation and Backward Locomotion

To study whether CEPsh glia affect AVE activity, we generated animals expressing the fluorescent calcium reporter GCaMP in AVE and confined them to a narrow trap in which they were able to move their head for short distances back and forth (Chronis et al., 2007). In this assay, frequent changes in AVE calcium levels and in head position are observed (Figures S4A and S4B; Movie S3). We classified AVE activity into four states, ramping up, ramping down, and high or low plateaus, and analyzed the transition between these states using a Hidden Markov Model (Figures S4C and S4D) (Kato et al., 2015). This analysis revealed a strong correlation between calcium increases in AVE and backward retraction of the head in wild-type animals (Figures 4A–4C). Calcium increases in AVE were previously shown to correlate with reversal movements (Kawano et al., 2011), suggesting that head retraction in our device likely indicates an intended reversal attempt. Importantly, the association between head movement and calcium activity is degraded in CEPsh glia-ablated animals (Figure 4B). Indeed, in CEPsh glia-ablated animals, >20% of calcium events are not accompanied by backward head retractions at all (error events; Figures 4C, S4E, and S4F). Moreover, while CEPsh glia-ablated and wild-type animals exhibit similar average AVE calcium amplitudes (Figure 4A) and frequencies (Figure S4G), the fraction of time AVE is in an active (on) state is significantly increased in CEPsh glia-ablated animals (Figure 4D).

To determine whether changes in AVE calcium dynamics are related to the ALA-AVE synapses ensheathed by CEPsh glia, we assayed AVE calcium activity in CEPsh glia-ablated animals carrying the *ceh-17* mutation. As shown in Figures 4A–4D, ALA inhibition is sufficient to restore normal AVE calcium peak duration and correlation with head movement to CEPsh glia-ablated animals. Thus, CEPsh glia control of AVE functional output requires ALA.

We wondered whether the prolonged calcium peaks and the decoupling of AVE activation from backward head movement are related defects. To test this, we examined AVE calcium levels in animals expressing tetanus toxin in AVE. We found that, by blocking AVE synaptic release, the mean duration of calcium signals is prolonged, as with CEPsh glia-ablated animals (Figure 4D). These results suggest that the prolonged AVE calcium peaks observed in CEPsh glia-ablated animals could be a result of inhibition of AVE synaptic output.

Our data suggest that the synapses between ALA and AVE are unusual. Activation of these inhibitory synapses blocks AVE output, but not by reducing AVE excitability, as the frequency and amplitude of AVE calcium peaks are not perturbed in CEPsh glia-ablated animals. We wondered, therefore, whether standard neurotransmitter signaling occurs at ALA-AVE synapses. We examined mutations in different neurotransmitter and neuropeptide pathways and assessed whether these can rescue the ectopic pausing episodes of adult CEPsh-ablated animals, as do mutations in *ceh-17* or ALA ablation. Some mutants we tested confer pausing behavior independently of glia ablation. For these, we assessed the ability to rescue the developmental delay of CEPsh-ablated animals. As summarized in Table S1, mutations affecting dopamine (*cat-2*), serotonin (*tph-1*), and glutamate (*eat-4*) signaling fail to rescue pausing, as does a mutation in *snf-11*, the transporter required for GABA accumulation in ALA (Gendrel et al., 2016). Acetylcholine (ACh) mutants could not be tested, as they exhibit greatly reduced locomotion and

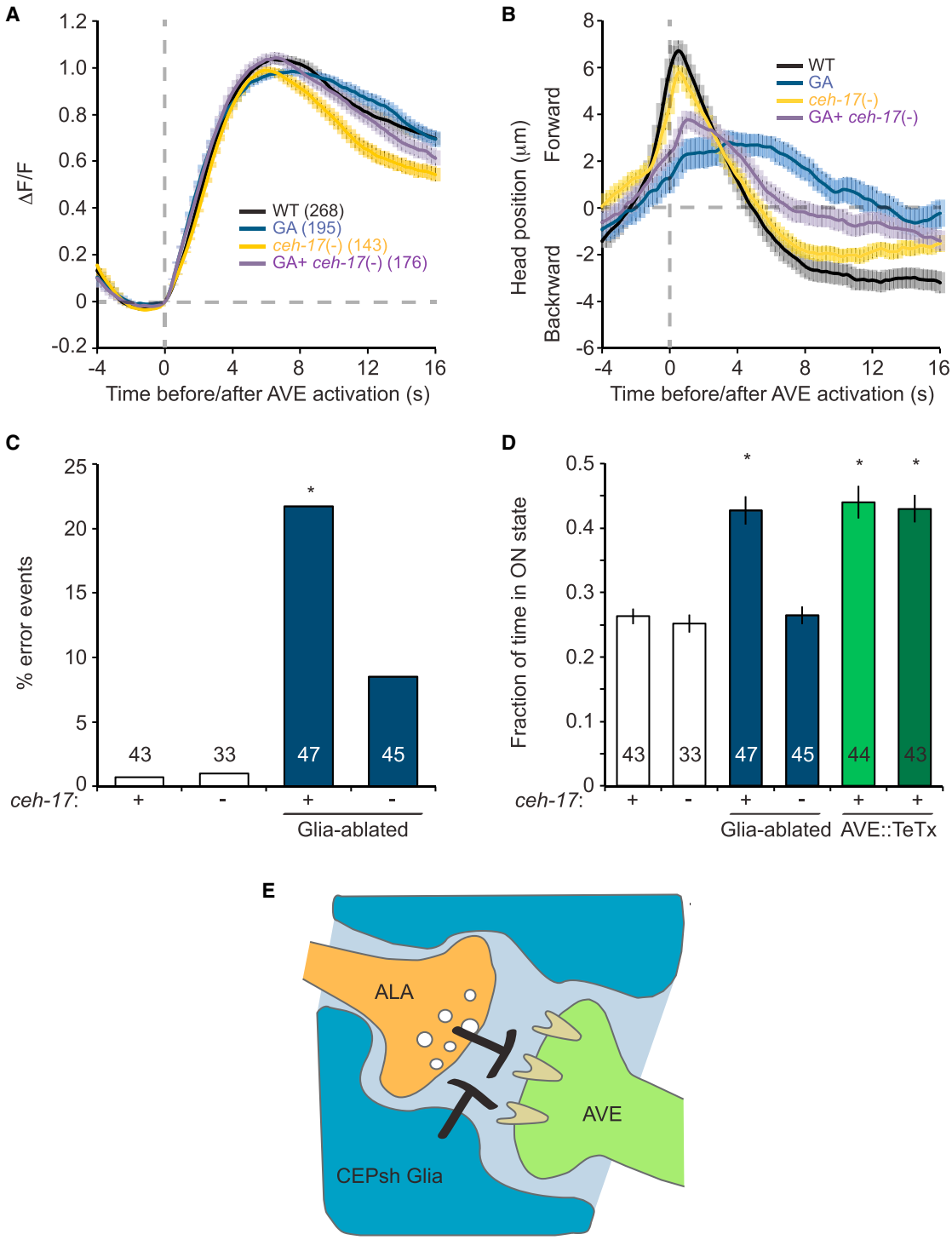

Figure 4. CEPsh Glia and ALA Affect AVE Calcium Signal Duration and Behavioral Output

(A) Average of AVE GCaMP signals, the number of total events analyzed for each strain is indicated on the graph. Dashed gray line, GCaMP signal rise initiation. All strains contain a GCaMP2.2 transgene.

(B) Head position relative to AVE GCaMP signal rise initiation (dashed gray line). Forward and backward head locations were determined by AVE cell body position.

(C) Percentage of events in which AVE GCaMP signal increase is not followed by backward head movement. Number of animals is indicated within or above each bar. (A–C) Error bars, mean ± SEM.

(legend continued on next page)

strong developmental delays; however, ALA does not express canonical ACh synthesis or uptake proteins (Pereira et al., 2015). Thus, ACh is likely not involved.

To examine the involvement of neuropeptide signaling, we tested mutations in genes controlling dense-core vesicle fusion (*unc-31* and *ida-1*) or neuropeptide maturation (*egl-21*/carboxypeptidase E and *aex-5*, *egl-3*, *kpc-1*, and *bli-4* peptide convertases). Only *aex-5* mutants show moderate rescue, possibly suggesting the involvement of neuropeptide signaling. We therefore examined mutations in neuropeptide/receptor genes that are highly enriched in ALA (Nath et al., 2016) or that have been previously associated with sleep regulation (*flp-7*, *flp-13*, *flp-24*, *nlp-8*, Nath et al., 2016; sNPF/*flp-27*, Shang et al., 2013; and *npr-22* implicated in the response of ALA to the RIS-released neuropeptide FLP-11, Turek et al., 2016). However, no suppression of CEPsh glia ablation defects was found. Pausing is markedly reduced by mutation in *npr-1*, a neuropeptide Y receptor implicated in lethargus (Choi et al., 2013). However, we found that NPR-1 expression in sensory neurons (Choi et al., 2013) is sufficient to restore ectopic pausing (Table S1), indicating that, at least in part, neuropeptide signaling can function upstream of the ALA-AVE synapse to control ectopic pausing.

Our results, therefore, eliminate most non-peptidergic neurotransmitter pathways as relevant for ALA-AVE synaptic function and suggest that either unknown *aex-5*-dependent neuropeptides or non-canonical signals mediate AVE synaptic inhibition by ALA.

DISCUSSION

Except for dwelling episodes associated with food (Fujiwara et al., 2002), stress (Hill et al., 2014), and molting (Raizen et al., 2008), the free-living nematode *C. elegans* continually moves. Here, we find that CEPsh glia of this animal control the transition into locomotion quiescence in the context of sleep. Importantly, glia are involved in sleep regulation in mice (Halassa et al., 2009; Pelluru et al., 2016) and flies (Seugnet et al., 2011), indicating an evolutionarily conserved function for this cell class.

Our results suggest a model (Figure 4E) in which CEPsh glia block an inhibitory synapse between the ALA and AVE neurons. Removal of CEPsh glia allows ALA to promote AVE inactivation, not by hyperpolarizing AVE but by uncoupling its synaptic input from its synaptic output.

Loss of CEPsh glia results in precocious episodes of quiescence immediately preceding lethargus in an ALA neuron-dependent manner. This unusual quiescence profile raises the possibility that sleep initiation may be governed by a gradual accumulation of sleep factors past a threshold, driving quiescence. Glia can serve to uptake a variety of neurotransmitters and secreted proteins from their surroundings (Conti et al., 2004; Rothstein et al., 1996), and it could therefore be that secreted moieties are relevant sleep factors. In this scenario, in CEPsh glia-ablated animals, the threshold for sleep entry is lowered by ectopic accumulation of sleep-inducing factors, resulting in premature sleep onset. Such a model may also explain the slower recovery from lethargus in CEPsh glia-ablated animals. A threshold model predicts that other sleep factors independent of CEPsh glia exist, as pre-lethargus quiescence episodes are transient and not consolidated as the main lethargus bout. Supporting this prediction, the ALA-dependent narcoleptic-like pausing behavior in CEPsh glia-ablated adults uncouples locomotion quiescence from other aspects of sleep, such as pharyngeal pumping. These findings not only suggest that sleep is a sum of different processes controlled by different pathways, but also implicate CEPsh glia and the ALA-AVE synapses they ensheath specifically in locomotion quiescence.

Only one other synaptic pairing is documented to be tightly ensheathed by CEPsh glia. This pairing, between the AIN and BAG presynaptic and postsynaptic neurons (White et al., 1986), is not known to have roles in sleep control. Nonetheless, the tight ensheathment may reflect an important synaptic function for glia that is not needed elsewhere. Indeed, our studies suggest that the ALA-AVE synapses may be atypical in other ways. Loss of CEPsh glia perturbs AVE functional output (reversal movement) in a manner dependent on ALA, but it affects neither the amplitude nor the frequency of AVE activation in our experimental setup. Such uncoupling of calcium induction and synaptic output has been previously reported in the ASER neuron of *C. elegans* in the context of a simple learning behavior. In that work, salt, which is usually attractive, becomes aversive when paired with starvation. Imaging of ASER reveals that salt cues usually induce calcium signals that drive synaptic vesicle release. Following starvation, however, neuronal outputs are inhibited even though calcium signals are enhanced (Oda et al., 2011). Thus, in addition to exhibiting uncoupling of synaptic input and output, inhibition of ASER by starvation and of AVE by CEPsh glia ablation are associated with increased calcium signal in these cells, suggesting the possibility of common, yet still unknown, underlying mechanisms.

It is of note that the ALA-AVE synapses are the most cell body-proximal synapses on AVE neurites (White et al., 1986). Whether this anatomical configuration reflects on the mechanism by which synaptic input and output are uncoupled in this neuron is unclear. Understanding the molecular nature of ALA-AVE neurotransmission should greatly aid in understanding how CEPsh glia inhibition of this synapse works. We have been able to eliminate most neurotransmitter classes and some ALA-expressed neuropeptides; however, peptidergic transmitters could still be relevant.

Finally, whether CEPsh glial activities in the context of sleep are dynamically modulated or whether these cells establish a fixed set point for neuronal activity that is not altered during the animal's life remains unknown. Identification of mediators of glial function and assessment of temporal changes in their activities, or lack thereof, will allow this question to be addressed.

(D) The mean fraction of the time AVE calcium signal is at the high plateau "on" state (Experimental Procedures) is prolonged in CEPsh-ablated and AVE-TeTx animals. Number of animals is indicated within or above each bar. (C and D) *$p < 0.01$, random permutation test.
(E) Model for CEPsh glia function. CEPsh glia negatively regulate the inhibitory signaling between ALA and AVE.
See also Figure S4.

EXPERIMENTAL PROCEDURES

For strains and plasmids used in this study as well as detailed descriptions of GFP reconstitution across synaptic partners (GRASP) signal acquisition and scoring, cell ablation, and development scoring, see the Supplemental Experimental Procedures.

Locomotion Analysis

First-day adults were washed off food and transferred to a 6-cm nematode growth media (NGM)-agar plate with a high-osmolarity barrier (4M Fructose) at the plate periphery to prevent wandering of animals off the plate. Animals were allowed to adjust to the plate for 20 min, and locomotion was recorded using a camera for 30 min at 2 frame/s. Custom Java scripts identified and tracked moving animals and analyzed worm pausing behaviors (see the Supplemental Experimental Procedures for more details). The fraction of the total time animals were found pausing in all tracks relative to the overall duration of all the tracks in a movie was used to calculate the percentage of time adult animals spent pausing.

Lethargus Behavior

Intermolt and lethargus quiescence assays were performed in artificial dirt polydimethylsiloxane (PDMS) chips as previously described (Iwanir et al., 2013), except that mid-L4 larvae were picked from a population of mixed-stage animals according to their morphology, and behavior was recorded for 10 hr. Generally, the onset of lethargus was defined as the first time point from which the fraction of quiescence remained above 5% for 20 consecutive min; for animals displaying substantial pre-lethargic quiescence, the starting point for the quiescence threshold search was determined manually based on the quiescence profile (see the Supplemental Experimental Procedures for more details).

Analysis of AVE Activity and Response

Calcium imaging from the AVE neuron was performed using a microfluidic device as described (Chronis et al., 2007). Images were captured for 5 min at 4 frames/s and analyzed using a custom Java code for AVE activity and position within the microfluidic device (see the Supplemental Experimental Procedures for more details).

Statistics

ANOVA Tukey's honest significant difference (HSD) post hoc test was used in the behavioral and developmental assays for comparison of multiple populations of animals using an R script with the null hypothesis that all samples are similar. Random permutation tests were used to evaluate the significance of differences in AVE activity and worm response between worm populations, using a Java code. Consider two sets of recordings from individual worms, n_1 from population 1 and n_2 from population 2. Each recording, which can comprise multiple AVE activation events, is treated as an independent sample. To test the null hypothesis that the two worm populations are equivalent, a large number (10^5) of random rearrangements of the two sets of samples into two groups of sizes n_1 and n_2 is generated. The stated significance figures are obtained as the fraction of the rearrangements for which the difference in the quantity of interest (fraction of error events or fraction of the time in the "on" state) between the rearranged groups is at least as large as the difference between the original groups. Unpaired two-sided Student's t test was used to determine the statistical significance between glia-ablated and non-ablated animals that are mutated for the various neurotransmitter and neuropeptide pathways.

SUPPLEMENTAL INFORMATION

Supplemental Information includes Supplemental Experimental Procedures, four figures, one table, and three movies and can be found with this article online at https://doi.org/10.1016/j.celrep.2018.02.036.

ACKNOWLEDGMENTS

We thank Daniel Colón-Ramos, Kang Shen, Cori Bargmann, Cheryl Van Buskirk, and the *Caenorhabditis* Genetic Center (CGC) (NIH P40 OD010440) for strains and reagents and the Shaham lab for comments and discussions. This work was supported by EMBO fellowship ALTD 870-200 to M.K. and by NIH grants NS095795 and NS064273 to S.S.

AUTHOR CONTRIBUTIONS

M.K. and S.S. designed experiments, interpreted data, and wrote the manuscript. F.C. developed the worm tracking and locomotion analysis code and analyzed the calcium kinetics studies. S.I. and D.B. developed the code for analysis of lethargus behavior. S.I. analyzed the lethargus behavior. M.K. conducted all experiments.

DECLARATION OF INTERESTS

The authors declare no competing interests.

Received: November 7, 2017
Revised: January 16, 2018
Accepted: February 8, 2018
Published: March 6, 2018

REFERENCES

Aida, T., Yoshida, J., Nomura, M., Tanimura, A., Iino, Y., Soma, M., Bai, N., Ito, Y., Cui, W., Aizawa, H., et al. (2015). Astroglial glutamate transporter deficiency increases synaptic excitability and leads to pathological repetitive behaviors in mice. Neuropsychopharmacology *40*, 1569–1579.

Barca-Mayo, O., Pons-Espinal, M., Follert, P., Armirotti, A., Berdondini, L., and De Pietri Tonelli, D. (2017). Astrocyte deletion of Bmal1 alters daily locomotor activity and cognitive functions via GABA signalling. Nat. Commun. *8*, 14336.

Brancaccio, M., Patton, A.P., Chesham, J.E., Maywood, E.S., and Hastings, M.H. (2017). Astrocytes Control Circadian Timekeeping in the Suprachiasmatic Nucleus via Glutamatergic Signaling. Neuron *93*, 1420–1435.e5.

Brown, R.E., Basheer, R., McKenna, J.T., Strecker, R.E., and McCarley, R.W. (2012). Control of sleep and wakefulness. Physiol. Rev. *92*, 1087–1187.

Chalfie, M., Sulston, J.E., White, J.G., Southgate, E., Thomson, J.N., and Brenner, S. (1985). The neural circuit for touch sensitivity in Caenorhabditis elegans. J. Neurosci. *5*, 956–964.

Chelur, D.S., and Chalfie, M. (2007). Targeted cell killing by reconstituted caspases. Proc. Natl. Acad. Sci. USA *104*, 2283–2288.

Cho, J.Y., and Sternberg, P.W. (2014). Multilevel modulation of a sensory motor circuit during C. elegans sleep and arousal. Cell *156*, 249–260.

Choi, S., Chatzigeorgiou, M., Taylor, K.P., Schafer, W.R., and Kaplan, J.M. (2013). Analysis of NPR-1 reveals a circuit mechanism for behavioral quiescence in C. elegans. Neuron *78*, 869–880.

Chronis, N., Zimmer, M., and Bargmann, C.I. (2007). Microfluidics for in vivo imaging of neuronal and behavioral activity in Caenorhabditis elegans. Nat. Methods *4*, 727–731.

Colón-Ramos, D.A., Margeta, M.A., and Shen, K. (2007). Glia promote local synaptogenesis through UNC-6 (netrin) signaling in C. elegans. Science *318*, 103–106.

Conti, F., Minelli, A., and Melone, M. (2004). GABA transporters in the mammalian cerebral cortex: localization, development and pathological implications. Brain Res. Brain Res. Rev. *45*, 196–212.

Eroglu, C., and Barres, B.A. (2010). Regulation of synaptic connectivity by glia. Nature *468*, 223–231.

Feinberg, E.H., Vanhoven, M.K., Bendesky, A., Wang, G., Fetter, R.D., Shen, K., and Bargmann, C.I. (2008). GFP Reconstitution Across Synaptic Partners (GRASP) defines cell contacts and synapses in living nervous systems. Neuron *57*, 353–363.

Fry, A.L., Laboy, J.T., and Norman, K.R. (2014). VAV-1 acts in a single interneuron to inhibit motor circuit activity in Caenorhabditis elegans. Nat. Commun. *5*, 5579.

Fujiwara, M., Sengupta, P., and McIntire, S.L. (2002). Regulation of body size and behavioral state of C. elegans by sensory perception and the EGL-4 cGMP-dependent protein kinase. Neuron *36*, 1091–1102.

García-Marín, V., García-López, P., and Freire, M. (2007). Cajal's contributions to glia research. Trends Neurosci. *30*, 479–487.

Gendrel, M., Atlas, E.G., and Hobert, O. (2016). A cellular and regulatory map of the GABAergic nervous system of C. elegans. eLife *5*, e17686.

Halassa, M.M., Fellin, T., and Haydon, P.G. (2007). The tripartite synapse: roles for gliotransmission in health and disease. Trends Mol. Med. *13*, 54–63.

Halassa, M.M., Florian, C., Fellin, T., Munoz, J.R., Lee, S.Y., Abel, T., Haydon, P.G., and Frank, M.G. (2009). Astrocytic modulation of sleep homeostasis and cognitive consequences of sleep loss. Neuron *61*, 213–219.

Hill, A.J., Mansfield, R., Lopez, J.M., Raizen, D.M., and Van Buskirk, C. (2014). Cellular stress induces a protective sleep-like state in C. elegans. Curr. Biol. *24*, 2399–2405.

Iwanir, S., Tramm, N., Nagy, S., Wright, C., Ish, D., and Biron, D. (2013). The microarchitecture of C. elegans behavior during lethargus: homeostatic bout dynamics, a typical body posture, and regulation by a central neuron. Sleep (Basel) *36*, 385–395.

Jeon, M., Gardner, H.F., Miller, E.A., Deshler, J., and Rougvie, A.E. (1999). Similarity of the C. elegans developmental timing protein LIN-42 to circadian rhythm proteins. Science *286*, 1141–1146.

Kato, S., Kaplan, H.S., Schrödel, T., Skora, S., Lindsay, T.H., Yemini, E., Lockery, S., and Zimmer, M. (2015). Global brain dynamics embed the motor command sequence of Caenorhabditis elegans. Cell *163*, 656–669.

Kawano, T., Po, M.D., Gao, S., Leung, G., Ryu, W.S., and Zhen, M. (2011). An imbalancing act: gap junctions reduce the backward motor circuit activity to bias C. elegans for forward locomotion. Neuron *72*, 572–586.

Krueger, J.M., Rector, D.M., Roy, S., Van Dongen, H.P., Belenky, G., and Panksepp, J. (2008). Sleep as a fundamental property of neuronal assemblies. Nat. Rev. Neurosci. *9*, 910–919.

Monsalve, G.C., Van Buskirk, C., and Frand, A.R. (2011). LIN-42/PERIOD controls cyclical and developmental progression of C. elegans molts. Curr. Biol. *21*, 2033–2045.

Nagy, S., Tramm, N., Sanders, J., Iwanir, S., Shirley, I.A., Levine, E., and Biron, D. (2014). Homeostasis in C. elegans sleep is characterized by two behaviorally and genetically distinct mechanisms. eLife *3*, e04380.

Nath, R.D., Chow, E.S., Wang, H., Schwarz, E.M., and Sternberg, P.W. (2016). C. elegans Stress-Induced Sleep Emerges from the Collective Action of Multiple Neuropeptides. Curr. Biol. *26*, 2446–2455.

Nelson, M.D., Trojanowski, N.F., George-Raizen, J.B., Smith, C.J., Yu, C.C., Fang-Yen, C., and Raizen, D.M. (2013). The neuropeptide NLP-22 regulates a sleep-like state in Caenorhabditis elegans. Nat. Commun. *4*, 2846.

Nelson, M.D., Lee, K.H., Churgin, M.A., Hill, A.J., Van Buskirk, C., Fang-Yen, C., and Raizen, D.M. (2014). FMRFamide-like FLP-13 neuropeptides promote quiescence following heat stress in Caenorhabditis elegans. Curr. Biol. *24*, 2406–2410.

Ng, F.S., Tangredi, M.M., and Jackson, F.R. (2011). Glial cells physiologically modulate clock neurons and circadian behavior in a calcium-dependent manner. Curr. Biol. *21*, 625–634.

Nichols, A.L.A., Eichler, T., Latham, R., and Zimmer, M. (2017). A global brain state underlies C. elegans sleep behavior. Science *356*, eaam6851.

Oda, S., Tomioka, M., and Iino, Y. (2011). Neuronal plasticity regulated by the insulin-like signaling pathway underlies salt chemotaxis learning in Caenorhabditis elegans. J. Neurophysiol. *106*, 301–308.

Ogata, K., and Kosaka, T. (2002). Structural and quantitative analysis of astrocytes in the mouse hippocampus. Neuroscience *113*, 221–233.

Pelluru, D., Konadhode, R.R., Bhat, N.R., and Shiromani, P.J. (2016). Optogenetic stimulation of astrocytes in the posterior hypothalamus increases sleep at night in C57BL/6J mice. Eur. J. Neurosci. *43*, 1298–1306.

Pereira, L., Kratsios, P., Serrano-Saiz, E., Sheftel, H., Mayo, A.E., Hall, D.H., White, J.G., LeBoeuf, B., Garcia, L.R., Alon, U., and Hobert, O. (2015). A cellular and regulatory map of the cholinergic nervous system of C. elegans. eLife *4*, e12432.

Poskanzer, K.E., and Yuste, R. (2016). Astrocytes regulate cortical state switching in vivo. Proc. Natl. Acad. Sci. USA *113*, E2675–E2684.

Pujol, N., Torregrossa, P., Ewbank, J.J., and Brunet, J.F. (2000). The homeodomain protein CePHOX2/CEH-17 controls antero-posterior axonal growth in C. elegans. Development *127*, 3361–3371.

Raizen, D.M., Zimmerman, J.E., Maycock, M.H., Ta, U.D., You, Y.J., Sundaram, M.V., and Pack, A.I. (2008). Lethargus is a Caenorhabditis elegans sleep-like state. Nature *451*, 569–572.

Ramón y Cajal, S. (1895). Algunas conjeturas sobre el mecanismo anatómico de la ideación, asociación y atención (Imprenta y Librería de Nicolás Moya).

Rapti, G., Li, C., Shan, A., Lu, Y., and Shaham, S. (2017). Glia initiate brain assembly through noncanonical Chimaerin-Furin axon guidance in C. elegans. Nat. Neurosci. *20*, 1350–1360.

Rothstein, J.D., Dykes-Hoberg, M., Pardo, C.A., Bristol, L.A., Jin, L., Kuncl, R.W., Kanai, Y., Hediger, M.A., Wang, Y., Schielke, J.P., and Welty, D.F. (1996). Knockout of glutamate transporters reveals a major role for astroglial transport in excitotoxicity and clearance of glutamate. Neuron *16*, 675–686.

Saper, C.B., Scammell, T.E., and Lu, J. (2005). Hypothalamic regulation of sleep and circadian rhythms. Nature *437*, 1257–1263.

Schwarz, J., Lewandrowski, I., and Bringmann, H. (2011). Reduced activity of a sensory neuron during a sleep-like state in Caenorhabditis elegans. Curr. Biol. *21*, R983–R984.

Seugnet, L., Suzuki, Y., Merlin, G., Gottschalk, L., Duntley, S.P., and Shaw, P.J. (2011). Notch signaling modulates sleep homeostasis and learning after sleep deprivation in Drosophila. Curr. Biol. *21*, 835–840.

Shang, Y., Donelson, N.C., Vecsey, C.G., Guo, F., Rosbash, M., and Griffith, L.C. (2013). Short neuropeptide F is a sleep-promoting inhibitory modulator. Neuron *80*, 171–183.

Singh, K., Chao, M.Y., Somers, G.A., Komatsu, H., Corkins, M.E., Larkins-Ford, J., Tucey, T., Dionne, H.M., Walsh, M.B., Beaumont, E.K., et al. (2011). C. elegans Notch signaling regulates adult chemosensory response and larval molting quiescence. Curr. Biol. *21*, 825–834.

Trojanowski, N.F., Nelson, M.D., Flavell, S.W., Fang-Yen, C., and Raizen, D.M. (2015). Distinct Mechanisms Underlie Quiescence during Two Caenorhabditis elegans Sleep-Like States. J. Neurosci. *35*, 14571–14584.

Tso, C.F., Simon, T., Greenlaw, A.C., Puri, T., Mieda, M., and Herzog, E.D. (2017). Astrocytes Regulate Daily Rhythms in the Suprachiasmatic Nucleus and Behavior. Curr. Biol. *27*, 1055–1061.

Turek, M., Lewandrowski, I., and Bringmann, H. (2013). An AP2 transcription factor is required for a sleep-active neuron to induce sleep-like quiescence in C. elegans. Curr. Biol. *23*, 2215–2223.

Turek, M., Besseling, J., Spies, J.P., König, S., and Bringmann, H. (2016). Sleep-active neuron specification and sleep induction require FLP-11 neuropeptides to systemically induce sleep. eLife *5*, e12499.

Van Buskirk, C., and Sternberg, P.W. (2007). Epidermal growth factor signaling induces behavioral quiescence in Caenorhabditis elegans. Nat. Neurosci. *10*, 1300–1307.

White, J.G., Southgate, E., Thomson, J.N., and Brenner, S. (1986). The structure of the nervous system of the nematode Caenorhabditis elegans. Philos. Trans. R. Soc. Lond. B Biol. Sci. *314*, 1–340.

Zhang, Y., Chen, K., Sloan, S.A., Bennett, M.L., Scholze, A.R., O'Keeffe, S., Phatnani, H.P., Guarnieri, P., Caneda, C., Ruderisch, N., et al. (2014). An RNA-sequencing transcriptome and splicing database of glia, neurons, and vascular cells of the cerebral cortex. J. Neurosci. *34*, 11929–11947.

Zimmerman, J.E., Naidoo, N., Raizen, D.M., and Pack, A.I. (2008). Conservation of sleep: insights from non-mammalian model systems. Trends Neurosci. *31*, 371–376.

Cell Reports, Volume *22*

Supplemental Information

Glia Modulate a Neuronal Circuit for Locomotion Suppression during Sleep in *C. elegans*

Menachem Katz, Francis Corson, Shachar Iwanir, David Biron, and Shai Shaham

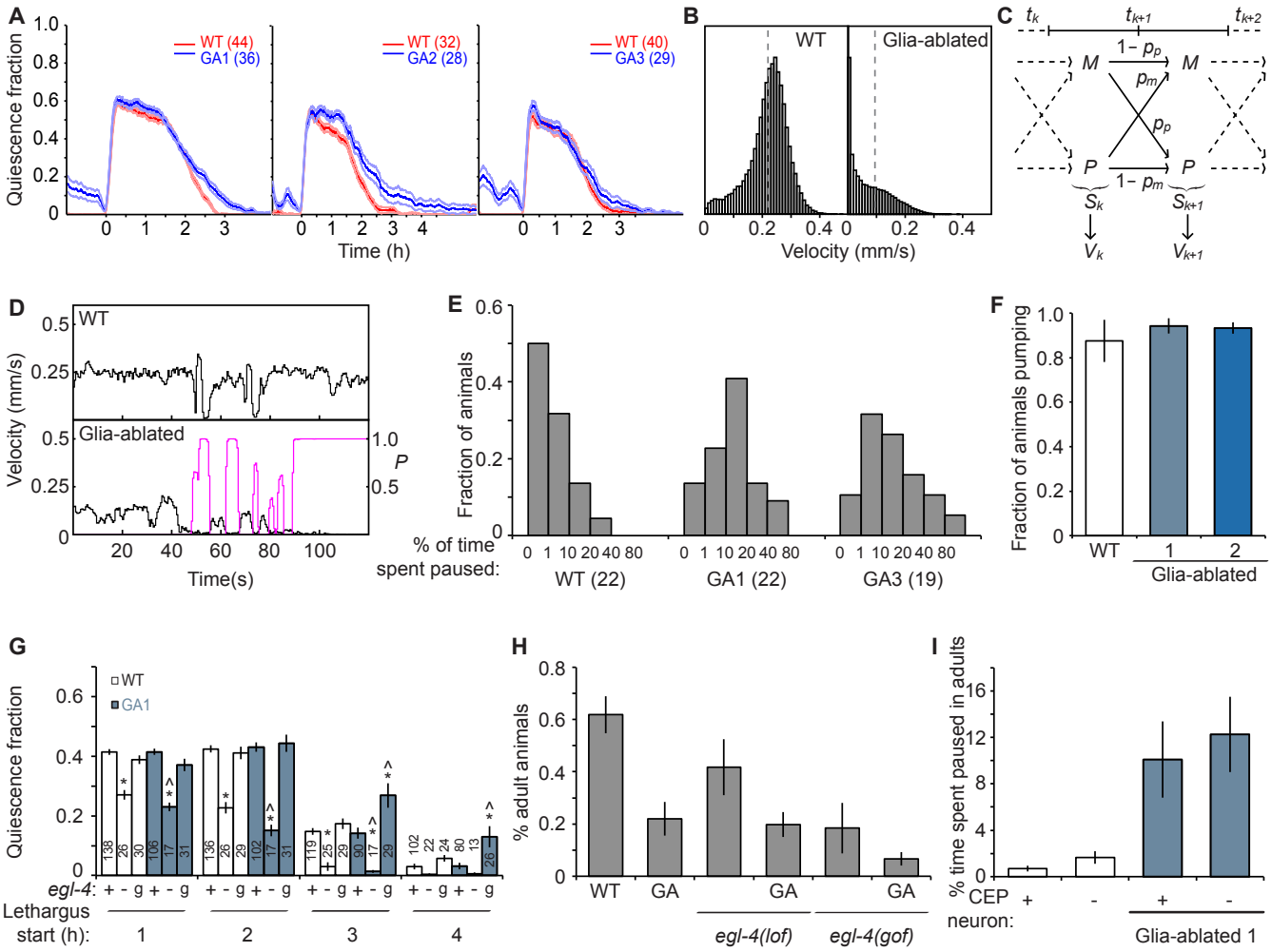

Figure S1. Related to Figure 1.

(A) Average quiescence fraction prior and during lethargus. WT, wild type. GA, glia ablated. Error bars indicate standard error. Number of animals is indicated in each panel.

(B) Velocity distribution of wild-type (WT) and glia-ablated worms.

(C) Hidden Markov Model for worm movement. S_k denotes the state of the worm (moving, *M*, or paused, *P*) in the time interval $[t_k, t_{k+1}]$ between frames *k* and *k*+1. The probabilities of transitions between the two states at each time step are shown by arrows. In each interval between two frames, the hidden state S_k determines the distribution of the observable velocity, V_k.

(D) Analysis of pausing from velocity curves. The instantaneous velocity of the animal is shown in black and the probability that the animal is paused in magenta. (Top) Wild-type worm (WT). Short periods of low velocity (corresponding to reversals and omega-turns) are not identified as pauses. (Bottom) Glia-ablated animal. The animal is initially moving then enters an extended period of pausing. As is often observed, short periods of pausing and slow movement alternate before an extended pause.

(E) Distribution of the percentage of time individual animals are pausing. Number of animals tested is indicated in parentheses below the graph.

(F) CEPsh glia ablation does not inhibit pumping in adults (four repeats).

(G) EGL-4 mutants affect the magnitude of sleep in wild type (WT) and glia-ablated (GA1) animals. *egl-4* loss-of-function mutation, -, gain-of-function mutation, g. Number of animals indicated inside or above bars.

(H) Percent animals reaching adulthood 52 hours after embryos are laid. Experiments are done in triplicate.

(I) Ablation of CEP neurons (-) does not induce locomotory pauses, nor does it suppress pausing of CEPsh-ablated animals (n=2 movies each). Vertical axis, the percentage of total time animals spent pausing out of the total duration of all recorded tracks.

(F-I) Graphs, mean ± s.e.m.; (G) ANOVA Tukey's HSD post hoc test, * compared to WT, ^ compared glia-ablated parent, $p<0.05$.

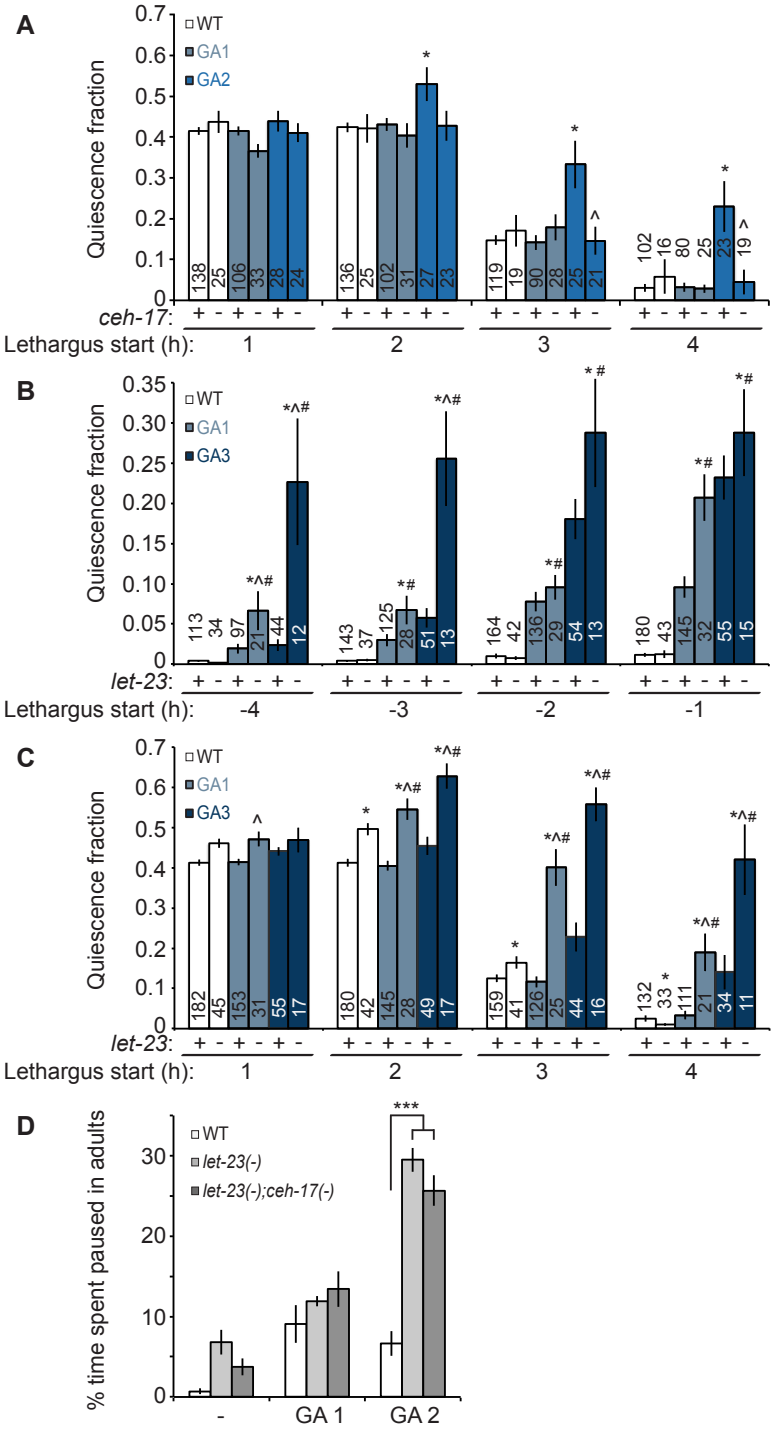

Figure S2. Related to Figure 2.

(A) *ceh-17* mutant **(-)** can rescue enhanced lethargus of CEPsh glia-ablated (GA) animals. Number of animals is indicated inside or above bars.

(B-D) A *let-23* mutation (-) enhances sleep defects of CEPsh glia-ablated animals before (B) and after (C) entry into lethagus, as well as pausing (D; n= 4 movies). Bar graphs, mean ± s.e.m.; ANOVA Tukey's HSD post hoc test, ***** compared to WT, ^ compared glia-ablated parent*,* # compered to parental mutant; number of symbols represent (1) $p<0.05$, (3) $p<0.0005$.

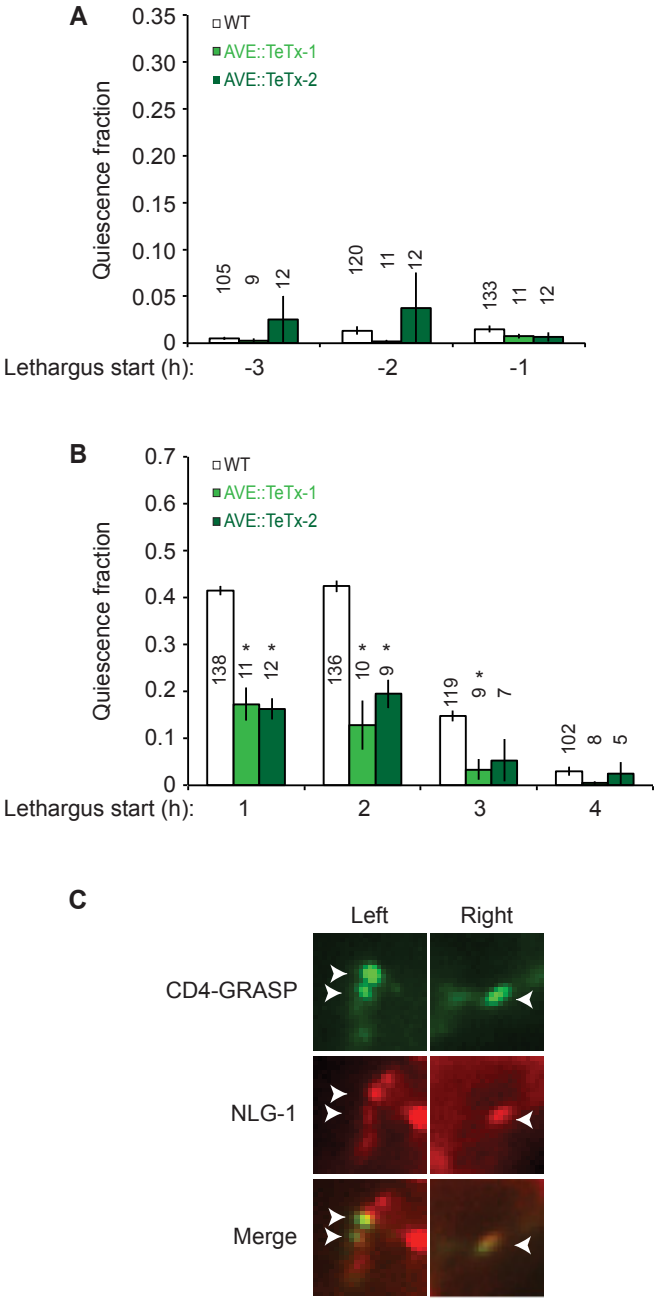

Figure S3. Related to Figure 3.

(A) Inhibition of AVE does not affect entry into lethargus. Number of animals is indicated above bars.

(B) AVE inhibition reduces lethargus quiescence. Number of animals is indicated inside or above bars.

(A,B) Bar graphs, mean ± s.e.m.; ANOVA Tukey's HSD post hoc test, * compared to WT, $p<0.05$.

(C) ALA-AVE synaptic contacts are maintained in CEPsh glia-ablated animals. ALA expresses CD4::spGFP11, and AVE expresses CD4::spGFP1-10, inactive GFP fragments that fluoresce when in close contact. Green signal corresponds to sites of contact. Neuroligin marks post-synaptic sites on AVE in red (NLG-1::mCherry). Synapses on both the left and the right sides of the nerve ring are presented.

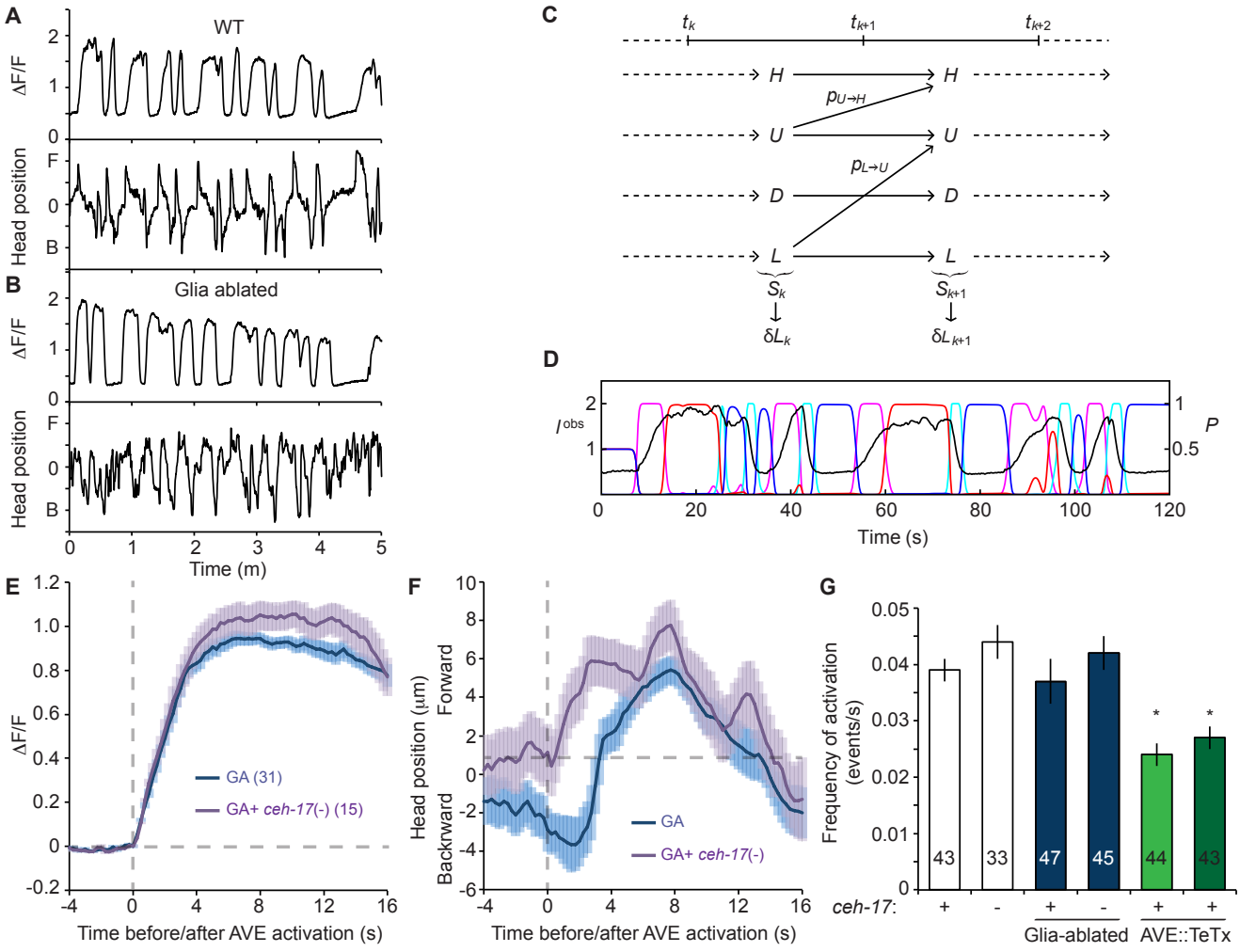

Figure S4. Related to Figure 4.

(A,B) Representative 5 minute recording of spontaneous GCaMP signals (top; Intensity/average intensity) and of head position (bottom), from a wild-type (WT; A) and a CEPsh glia-ablated animal (B).

(C) Hidden Markov Model for the analysis of neuron activity. The model comprises four activitystates, ramping up (*U*), ramping down (*D*), high plateau (*H*), and low plateau (*L*). The activity state S_k of the neuron in the time interval $[t_k, t_{k+1}]$ determines the distribution of the step δL_k in activity level between times t_k and t_{k+1}. For the sake of legibility, only two of the possible transitions between distinct activity states are shown, corresponding to the onset of neuron activity ($L \to U$) and to the stabilization of activity at a high level ($U \to H$). Some transitions (e.g. $U \to L$) are not permitted, in accordance with the natural meaning of the four activity states (only a decrease in activity can terminate in the low plateau state).

(D) Classification of activity states using a Hidden Markov Model. The measured activity level is plotted in black, while the colored curves show the probability of the different activity states, ramping up (magenta), ramping down (cyan), high plateau (red), and low plateau (dark blue).

(E,F) Average of AVE GCaMP signals (E), and head position (F) recorded from animals showing error responses. Dashed gray line, GCaMP signal rise initiation. The number of total events analyzed for each strain is indicated on the graph. Error bars, mean ± s.e.m.

(G) The frequency of AVE GCaMP activation events does not change in CEPsh-ablated animals, but is reduced by tetanus toxin expression in AVE. Error bars, mean ± s.e.m.; *, $p<0.01$, random permutation test. Number of animals is indicated within or above each bar.

Pausing					
Gene	**Allele**	**FC**	***p* value**	***n***	**ALA**
cat-2	*(e1112)*	1.02	0.9791	4	-
tph-1	*(mg280)*	0.78	0.7832	4	-
eat-4	*(ky5)*	1.23	0.6250	4	0.15
snf-11	*(ok156)*	1.02	0.9591	12	0.37
kpc-1	*(gk8)*	1.11	0.7580	4	-
aex-5	***(gk419962)***	**0.31**	**0.0219**	**13**	**54.5**
egl-3	*(n150)*	1.28	0.3374	4	42
egl-21	*(n476)*	0.79	0.2154	17	55.9
ida-1	*(ok409)*	3.02	0.0011	8	41.3
nlp-8;flp-13;flp-24	*(ok1799);(tm2427);(gk3109)*	1.06	0.8270	10	>332
flp-7	*(ok2625)*	1.35	0.4052	4	4518.55
flp-27	*(tm4612)*	0.45	0.1531	8	40.13
flp-27	*(gk3331)*	2.58	0.0210	8	40.13
npr-22	*(ok1598)*	0.7	0.2503	10	-
npr-1	***(ad609)***	**0.14**	**0.0004**	**10**	**-**
npr-1+ rescue	*(ad609)+(kyEx1966)*	1.39	0.4918	4	

Developmental delay					
Gene	**Allele**	**FC**	***p* value**	***n***	**ALA**
unc-31	*(e928)*	1.15	0.0041	2	-
bli-4	*(e937)*	1.02	0.6280	2	4.23

Supplemental Table S1. Related to Figure 4.

Effect of mutations in neurotransmitter and neuropeptide pathways on CEPsh glia ablation-induced pausing (top), and developmental delay (bottom). FC, response fold change relative to CEPsh glia-ablated animals. *p* value, two tailed student's *t* test. *n*, number of movies analyzed or experimental replicates. ALA, gene expression levels in ALA according in RPKM (Nath et al., 2016).

Experimental Procedures

Strains

C. elegans strains were cultured at 20°C as described (Brenner, 1974), unless otherwise indicated. Wild-type (WT) animals were Bristol strain N2. Other alleles used in this work are:

IB16-*ceh-17(np1)I.* VC48- *kpc-1(gk8)I.* OS8656- *aex-5(gk419962)I* outcrossed x4. OS11077- *nlp-8(ok1799)I; flp-13(tm2427)III, flp-24(gk3109)III.* CB937- *bli-4(e937)I.* PS5131- *let-23(sy12)II.* CB1112-*cat-2(e1112)II.* MT15434- *tph-1(mg280)II.* VC2012- *flp-27(gk3331).* FX4612- *flp-27(tm4612)II* . OS9414-*eat-4(ky5)III* outcrossed x2. OS11752- *ida-1(ok409)III* outcrossed x1. FK234- *egl-4(ks62).* DA521- *egl-4(ad450)IV*. RB1405- *npr-22(ok1598)IV*. MT1071- *egl-21(n476)IV*. DA509- *unc-31(e928)IV* outcrossed x10. RM2710- *snf-11(ok156)V* outcrossed x6. MT150- *egl-3(n150)V* outcrossed x1. RB1990- *flp-7(ok2625)X.*

The following transgenic strains were used:

OS3537- *nsIs168* (P*hlh-17*::recCaspase-3, P*unc-122*::GFP, P*ptr-10*::myrRFP)

OS3549- *nsIs180* (P*hlh-17*::recCaspase-3, P*unc-122*::GFP)

OS3540- *nsIs171* (P*hlh-17*::recCaspase-3, P*unc-122*::GFP)

OS6243- *nsIs168; egl-4(ad450)*

OS6084- *nsIs168; egl-4(ks62)*

PS5803- P*ida-1*::GFP, *pha-1(e2123ts)*

OS4700- *nsIs168;* P*ida-1*::GFP

OS4882- *nsIs171; ceh-17(np1)*

OS4699- *nsIs168; ceh-17(np1)*

OS4762- *nsEx2714* (P*pept-3*::GFP, P*odr-1*::RFP)

OS4884- *nsIs168; nsEx2714*

OS4976- *nsEx2846* (P*pept-3*::TeTX, P*elt-2*::mCherry)

OS4977- *nsEx2847* (P*pept-3*::TeTX, P*elt-2*::mCherry)

OS5015- *nsEx2846*; *ceh-17(np1)*

OS5016- *nsEx2847*; *ceh-17(np1)*

OS6265- *nsEx2941* (P*ver-3*(700bp)::CD4-spGFP11, Coloem::dsRed); *nsEx2943* (P*pept-3*::CD4-spGFP1-10, P*elt-2*::mCherry); *nsEx3485* (P*pept-3*::NLG-1::mCherry, *rol-6(+)*)

OS6039- *nsEx3358* (P*pept-3*::GCaMP2.2, P*unc-122*::dsRed)

OS6261- *nsIs180; nsEx3358*

OS6615- *nsEx3358; ceh-17(np1)*

OS6617- *nsIs180; nsEx3358; ceh-17(np1)*

OS6851- *nsEx3737* (P*pept-3*::TeTX-sl2-GCaMP2.2, P*unc-122*::dsRed)

OS6858- *nsEx3744* (P*pept-3*::TeTX-sl2-GCaMP2.2, P*unc-122*::dsRed)

OS5012- *nsIs168; eat-4(ky5)*

OS3981- *nsIs168; tph-1(mg280)*

OS9880- *nsIs168; snf-11(ok156)*

OS7750- *nsIs168; kpc-1(gk8)*

OS8697- *nsIs168; aex-5(gk419962).*

OS8698- *nsIs168; egl-3(n150)*

OS7401- *nsIs168; egl-21(n476)*

OS11084- *nsIs168; flp-13(tm2427), flp-24(gk3109); nlp-8(ok1799);*

OS7527- *nsIs168; flp-7(ok2625)*

OS7915- *nsIs168; flp-27(gk3331)*

OS8083- *nsIs168; flp-27(tm4612)*

OS7746- *nsIs168; npr-22(ok1598)*

CX9396- *npr-1(ad609); kyEx1966 (*P*flp-21::*NPR-1-sl2-GFP*,* P*ofm-1::*dsRed*)*

OS8085- *nsIs168; npr-1(ad609); kyEx1966 (*P*flp-21::*NPR-1-sl2-GFP*,* P*ofm-1::*dsRed*)*

OS7604- *nsIs168; unc-31(e928)*

OS9400- *nsIs168; bli-4(e937)*

OS11763- *nsIs168; ida-1(ok409)*

Germline transformations were performed as described (Mello and Fire, 1995). Stable transgenes were obtained via psoralen integration (Yandell et al., 1994).

Ablations

Laser ablations of the ALA, AVE and CEP neurons were performed as described (Bargmann and Avery, 1995) in L1 larvae of strains expressing GFP under the *ida-1, pept*-3 or the *dat-1* promoters, respectively, to assist in neuron identification. Ablated animals were selected for the behavioral experiments by absence of GFP. For genetic ablation of CEPsh glia, the two parts of a reconstituted Caspase-3 (Chelur and Chalfie, 2007) were expressed in CEPsh glia starting at the early L1 stage by using the *hlh-17* promoter (McMiller and Johnson, 2005). In all animals tested complete elimination of all four CEPsh glia in these strains was observed based on the lack of P*ptr-10::*myrRFP expression in the CEPsh cells (n>50), and also confirmed in two animals by EM reconstruction.

Analysis of animal locomotion

A day prior to behavior recordings, L4 larvae were picked to a fresh plate with food. The next day, 20-40 adult animals were picked to an unseeded plate, washed three times with M9 buffer, and transferred to a 6 cm plate containing 4 ml of NGM-agar, with a high-osmolarity barrier (4M Fructose) at the periphery of the plate to prevent wandering of animals off the plate. Animals were allowed to adjust to the plate for 20 minutes before the plate was placed under a video camera, and locomotion was recorded for 30 minutes at 2 frame/sec (Movies S1, 2). Animal locomotion was analyzed using custom software written in Java, as follows.

Worm tracking

Individual movie frames are first analyzed separately to determine worm positions. The background of each frame is computed using a median filter (65x65 pixels) and subtracted before further processing. A binary image is then obtained by thresholding; objects in the image are identified as the connected components of the foreground, and define groups of pixels in the background-subtracted image. The total intensity of an object is computed by summing the intensities of its pixels, and its center as the center of mass of its pixels (weighted by their intensities). Objects with a total intensity below a set threshold are discarded.

Objects in two consecutive frames are then matched if they have at least one pixel in common (the frame rate was sufficiently high that images of a worm in two consecutive frames always overlapped). This

defines a “trajectory graph” whose vertices are object centers in the different movie frames and whose edges connect matched objects in consecutive frames. Branches of the graph define candidate worm trajectories, which are then edited, automatically and manually, to remove spurious tracks. Firstly, worms can come in contact as they move around the plate, and occasionally remain alongside one another before they separate. These touching worms are incorrectly identified as a single object. However, encounters between worms are readily detected in the trajectory graph as two incoming branches merging into a single branch. The merged branch is then discarded. Conversely, a single branch that splits into two is identified as two adjacent worms that later separated, and discarded. Another source of spurious tracks are dust particles and damaged or dead worms. These immobile objects are detected as tracks that do not deviate from their average position by more than a threshold distance, and discarded. This automated processing eliminates most spurious tracks, so that limited subsequent manual editing is needed. A graphical interface was developed for that purpose, allowing the user to inspect tracking results and discard incorrect tracks.

Analysis of worm pausing

Worm trajectories were analyzed to identify periods of movement and pausing, according to the variations in worm velocity. To estimate the velocity of a worm, its trajectory is first smoothed by convolution with the kernel

$$h(k) = \frac{3^{-|k|}}{2}.$$

The velocity of the worm between frames k and k+1 is then defined as

$$v_k = \frac{\left\| \vec{r}_{k+1} - \vec{r}_k \right\|}{\Delta t},$$

where $\vec{r}_k$ denotes the position of the worm in frame k and Δt=0.5 s is the interval between frames.

This rapidly decaying kernel is chosen as a compromise between preserving rapid variations in worm velocity and reducing noise in the estimation of worm positions. The velocity of the worm between consecutive frames is estimated as the distance between points in the smoothed trajectory divided by the time interval Δt between frames.

Because pausing worms exhibit some residual movement and the velocity of moving worms can be small (e.g. when they are reversing), these two states cannot be discriminated based on instantaneous velocity; as seen in Figure S1B, the velocity distribution of glia-ablated worms does not have a clear bimodal structure. An improvement over velocity thresholding at each time point would be to require that the velocity remains above/below threshold for a minimum period of time. However, this would require introducing several somewhat arbitrary parameters and would be sensitive to noise. To explicitly allow for ambiguities in the identification of movement and pausing, trajectories were analyzed using a statistical model, specifically a Hidden Markov Model (Press, 2007).

The model, depicted in Figure S1C, comprises two states, moving and paused (denoted *M* and *P*). At each time step, a moving worm can pause with probability p_p and a paused worm can start moving with probability p_m. Thus, if S_k denotes the state of the worm in the interval between frames *k* and *k*+1,

$$p(S_{k+1} = M) = (1 - p_p)\, p(S_k = M) + p_m\, p(S_k = P),$$
$$p(S_{k+1} = P) = (1 - p_m)\, p(S_k = P) + p_p\, p(S_k = M).$$

The velocity of the worm depends on its state, and is assumed to follow a half-normal distribution with scale σ_M and σ_P for the moving and paused states, respectively:

$$p(V_k = v \mid S_k = M) \propto e^{-\frac{v^2}{2\sigma_M^2}},$$
$$p(V_k = v \mid S_k = P) \propto e^{-\frac{v^2}{2\sigma_P^2}}.$$

Note that this simple model is not intended to accurately represent the statistics of worm movement; instead, it formalizes minimal assumptions about movement and pausing, and allows their identification to be cast as an inference problem. That is, given an observed velocity sequence $\mathbf{v} = \{v_1, \ldots, v_n\}$, the model defines a likelihood (posterior probability) $P(\mathbf{s} \mid \mathbf{v})$ for every sequence of model states $\mathbf{s} \in \{M, P\}^n$, e.g. $\mathbf{s} = \{M, M, P, \cdots\}$. The probability that the worm was in the paused state in the interval between frames *k* and *k*+1 is the marginal probability $P(S_k = P \mid \mathbf{v})$. The forward-backward algorithm (Press, 2007) allows efficient computation of the likelihood of state sequences and other quantities of interest, such as the expectations of the time spent in each state and of the number of transitions between the two states. The transition probabilities p_p and p_m can thus be re-estimated from

the output of the algorithm. The Baum-Welch algorithm (Press, 2007; Welch, 2003) iterates rounds of the backward-forward algorithm and parameter re-estimation; the likelihood of the data under the model increases monotonically at each step, guaranteeing convergence to a maximum. Thus, transition probabilities are not free parameters of the model but estimated from the data.

This procedure was used to estimate transition probabilities for each analyzed movie (pooling all the tracks in the movie). On the other hand, the velocity scales σ_M = 150 μm/s and σ_P = 5 μm/s (which could also be re-estimated) were kept fixed for all movies, to ensure a consistent definition of the two states across all experiments; these values were determined from the analysis of a sample of movies of wild-type worms.

Figure S1D illustrates the output of this analysis. Because of the probabilistic nature of the model, transitions between states are not discrete but occur over a small number of time steps. Also, ambiguous features of the activity curve give rise to fractional probabilities. The fraction of the total time animals were found pausing in all tracks relative to the overall duration of all the tracks in a movie was used to calculate the percentage of time adult animals spent pausing.

Lethargus behavior assays

Intermolt and lethargus quiescence assays were performed in "artificial dirt" PDMS chips as previously described (Iwanir et al., 2013), except that mid L4 larvae were picked from a population of mixed stage animals according to their morphology, and behavior was recorded for 10 hours. For the traces in Figure 1A,B , the fraction of quiescence was calculated as described by (Iwanir et al., 2013) over a 10-minute running window. For statistical analysis of populations, the fraction of quiescence was discretely calculated for one-hour bins. Generally, the onset of lethargus was defined as the first time-point from which the fraction of quiescence remained above 5% for 20 consecutive minutes, for animals displaying substantial pre-lethargic quiescence, the starting point for the quiescence threshold search was determined manually based on the quiescence profile.

Statistical significance was tested using one-way ANOVA with Tukey-Kramer Correction on planned comparisons of the double mutants to each parent line, and each parent line to the wild type.

Scoring development

Ten gravid adult animals were allowed to lay eggs for 4 hours and removed from the plate. Animals were scored 55 hours later and placed into three groups, worms that reached adulthood, L4 larvae, and L1-L3 larvae. The percentage of animals in each group was calculated. The data shown is the average of three assays, with at least 150 worms scored in each assay.

Scoring synapses by GRASP

GRASP expressing lines were generated as described (Feinberg et al., 2008). Two individual lines, separately expressing the two parts of CD4-GRASP in ALA and AVE, were crossed together and specific expression of GFP within the nerve ring was confirmed. To verify that these neurons interact at synaptic sites, AVE synapses were marked with neuroligin (NLG-1::mCherry), and the percentage of animals with an overlapping red signal out of a population of animals with a clear GRASP signal was calculated. Fluorescence imaging was done using an Axioplan II microscope equipped with an AxioCam camera, using a 63x/1.4 NA objective. Figures were assembled using Photoshop (Adobe Software).

Calcium imaging

Calcium imaging from AVE neuron was performed using a microfluidic device as described (Chronis et al., 2007). Images were captured at 4 frames/sec and were analyzed using AxioVision 4.7.

Analysis of AVE activity and response

Images were first downsampled (from ≈ 0.1μm/pixel to 0.4μm/pixel) then processed as follows.

Neuron tracking

The location of the neuron in each movie frame is determined as a local maximum of the image after smoothing with a Gaussian filter (standard deviation of 4 pixels ≈ 1.6μm). The initial location is set to the absolute maximum in the first frame (or manually if this does not match the position of the neuron). Subsequently, the location in each frame is determined as the maximum within a distance *r* of the location in the previous frame (the default value of *r* was 32 pixels ≈ 13μm). This procedure tracked the neuron

correctly for the majority of movies, and for most others with the following adjustments. The value of *r* was increased (to 64 pixels) for movies in which motion exhibited sudden jumps (N=4/300). When other structures in the vicinity of the neuron interfered with the tracking, the value of *r* was reduced (to 16 pixels, provided motion was not too fast; N=17/300) and/or possible neuron positions were restricted to a manually defined rectangular area (N=9/300). For some movies, these adjustments were not sufficient to track the neuron correctly. These movies represented a limited fraction of all recordings (N=35/300) and were omitted from the analysis.

Estimation of neuron activity

At each time point, the activity of the neuron is estimated from pixel intensities in a circular area around the estimated neuron position. The radius of the area (20 pixels ≈ 8μm) is chosen to be as small as possible while sufficient to enclose the body of the neuron. The background intensity in the vicinity of the neuron is estimated as the median intensity in a ring-shaped domain with an inner radius of 20 pixels and an outer radius of 40 pixels. Finally, the activity of the neuron is estimated by summing over the inner circular area the pixel intensity minus the background level. For every movie, this value is divided by its time average, yielding a dimensionless measure of neuron activity. Examination of the resulting activity curves suggested variations in measurement noise (due e.g. to variations in imaging conditions). Curves that were deemed too noisy (based on an RMS variation in activity level > 0.1 between successive frames; N=10/265) were excluded from further analysis.

Analysis of neuron activity

Inspection of activity curves obtained for wild-type worms (e.g. Figure S4A) suggests that as was previously reported (Kato et al., 2015) they may be broken down into four states: ramping up, ramping down, and high or low plateaus (denoted *U*, *D*, *H*, and *L*, respectively). As for the analysis of worm locomotion, a Hidden Markov Model (depicted in Figure S4C) was used to classify neuron activity into these four states (here also, the model is not intended to represent the detailed statistics of neuron activity, but as a tool for its analysis).

Because reporter activity and the measurement process are noisy, it is not possible to directly use increments between successive time points to define the four states, unless the activity curves are strongly smoothed. On the other hand, this would blur the transitions between ramps and plateaus. To explicitly allow for uncertainty in the measurement of neuron activity, a hidden variable corresponding to the "true" activity level was incorporated into the model. For the purpose of inference, the range of possible activity levels is discretized into N evenly spaced values, $\{l_1,\cdots,l_N\}$ (N=128 is chosen such that the increment Δl between levels is smaller than the measurement noise). The model thus comprises $4N$ states, corresponding to all possible combinations of activity states (U, D, H, L) and activity levels.

At each time step, the possible transitions between model states include transitions between activity states and transitions between different activity levels. By definition, transitions between ramping up and low plateau are not permitted, as well as transitions between ramping down and high plateau and transitions between plateau states. Thus, if S_k denotes the activity state at time t_k and $p_{A\to B}$ denotes the probability of an allowed transition between activity states A and B,

$$P(S_{k+1}=U)=(1-p_{U\to H}-p_{U\to D})P(S_k=U)+p_{L\to U}P(S_k=L)+p_{D\to U}P(S_k=D).$$

Similar equations are obtained for the other three states.

Variations in the activity level depend on the activity state. By definition of the activity states, activity can only increase in the ramping up state or decrease in the ramping down state. Steps in activity in these two states are assumed to follow an exponential distribution with scale λ, e.g. if L_k denotes the activity level at time t_k,

$$P(L_{k+1}=l_j \mid L_k=l_i, S_k=U)\propto e^{-\frac{l_j-l_i}{\lambda}}.$$

The scale λ can be written as $\lambda=\rho\Delta t$, where ρ is the average rate of change of the activity level and $\Delta t=0.25\text{s}$ is the time step between movie frames.

Activity in the plateau states is assumed to be approximately constant, with small fluctuations only; transitions are allowed only between adjacent levels (among the N bins), with a small probability ε, e.g.

$$P(L_{k+1} = l_{i-1} \mid L_k = l_i, S_k = H) = \varepsilon,$$
$$P(L_{k+1} = l_i \mid L_k = l_i, S_k = H) = 1 - 2\varepsilon,$$
$$P(L_{k+1} = l_{i+1} \mid L_k = l_i, S_k = H) = \varepsilon.$$

This corresponds to a diffusive evolution with diffusivity

$$D = \varepsilon \frac{\Delta l^2}{\Delta t}.$$

Finally, the measurement of activity levels is assumed to be corrupted by Gaussian white noise with a variance σ^2, thus if l_k^{obs} denotes the level measured at time t_k,

$$P(l_k^{\text{obs}} \mid L_k = l_i) \propto e^{-\frac{(l_k^{\text{obs}} - l_i)^2}{2\sigma^2}}.$$

Given an observed activity sequence, $\mathbf{l}^{\text{obs}}$, the likelihood of state sequences, $P(\mathbf{s},\mathbf{l} \mid \mathbf{l}^{\text{obs}})$, is computed using the forward-backward algorithm. The rate of neuron activation is then obtained as the expected frequency of transitions to the ramping up state. Estimation of transition probabilities between activity states using the Baum-Welch algorithm was found to result in over-segmentation (high transition probabilities were obtained, with small jumps in activity being classified as transitions), thus their values were kept fixed. For simplicity, all allowed transitions were assigned the same probability *p*. This and the other model parameters were adjusted to values yielding satisfactory classification: $p = 0.01/\text{s}$, $\rho = 0.4/\text{s}$, $D = 2 \times 10^{-5}/\text{s}$, and $\sigma = 0.08$. Figure S4D illustrates the output of this procedure. As with the model of worm movement and pausing, transitions between states are not discrete but occur over a small number of time steps, and ambiguous features of the activity curve give rise to fractional probabilities (e.g. the shoulder in activity near *t*=90 is partly classified as a high plateau).

Analysis of the response to neuron activity

The above statistical model is well suited to count neuron activations, because there is a continuum from sharp onsets of activity to small jumps due to fluctuations in neuron activity and/or measurement noise. To assess the response of the worm to neuron activation, on the other hand, it is desirable to consider only the clearest activation events. To this end, discrete activation events are identified as time intervals where the

ramping up state has highest probability (among the four activity states), and the amplitude of an event is defined as the change in the measured activity level over the corresponding time interval; only events with an increment in ΔF/F above 0.6 are retained. Also, only those events which follow a low plateau (i.e. the low plateau state has the highest probably immediately before the start of the event) are considered, to ensure that the response to the activation event is separated from the response to prior down-steps in AVE activity. For each line, all events in the analyzed movies are pooled together to compute the average activity and worm position as a function of time (relative to event start time).

As shown in Figure 4B, wild-type worms respond to AVE activation by a sharp backward movement, while the response of glia-ablated worms is much less distinct. The strength of this phenotype is quantified according to the frequency with which worms move backward following neuron activation. To this end, the positions of the worm at two time points are compared. The first is the forward-most position of the worm within 2 seconds after the start of the activation event (this allows for the forward movement of wild-type worms between the start of the event and the onset of the response). The second time point is 8 seconds after the start of the event, corresponding to the typical duration of sharpest backward movement in wild-type worms. The response of the worm is measured by the difference *dx* in position between these two time points, and deemed "correct" or "incorrect" depending on whether the worm has moved backward ($dx < 0$) or forward ($dx > 0$). Because the movement of the worm is measured relative to the forward-most position in a 2-second interval after the start of the event, the resulting estimation of "error rates" is rather conservative: if it is computed using randomly drawn event times, an error rate of about 1/3 is obtained. The strength of the defect is measured relative to this randomized value, thus in the absence of any correlation between AVE activity and movement the defect has a strength of 1.

Plasmids

For specific expression in AVE, we PCR-amplified a 2.5 kbp genomic DNA fragment containing a sequence that ends 240 bp upstream of the *pept-3* ATG (Fei et al., 2000). *Fse*I and *Asc*I restriction sites were added on both sides of this amplicon, respectively. This fragment was ligated to the following vectors digested with the same enzymes: pSM-GFP; pSM-TeTx-mCherry; pSM-GCaMP2.2; pSM-NLG-1-mCherry; pSM-CD4-spGFP1-10.

For specific expression in ALA, we PCR-amplified a 650 bp genomic DNA fragment containing sequences upstream of the *ver-3* ATG (Popovici et al., 2002). The resulting amplicon was ligated to pSM-CD4-spGFP11 vector digested with *Fse*I and *Asc*I.

References

Bargmann, C.I., and Avery, L. (1995). Laser killing of cells in Caenorhabditis elegans. Methods Cell Biol. 48, 225-250.

Brenner, S. (1974). The genetics of Caenorhabditis elegans. Genetics 77, 71-94.

Chelur, D.S., and Chalfie, M. (2007). Targeted cell killing by reconstituted caspases. Proc. Natl. Acad. Sci. USA 104, 2283-2288.

Chronis, N., Zimmer, M., and Bargmann, C.I. (2007). Microfluidics for in vivo imaging of neuronal and behavioral activity in Caenorhabditis elegans. Nat. Methods 4, 727-731.

Fei, Y.J., Romero, M.F., Krause, M., Liu, J.C., Huang, W., Ganapathy, V., and Leibach, F.H. (2000). A novel H(+)-coupled oligopeptide transporter (OPT3) from Caenorhabditis elegans with a predominant function as a H(+) channel and an exclusive expression in neurons. J. Biol. Chem. 275, 9563-9571.

Feinberg, E.H., Vanhoven, M.K., Bendesky, A., Wang, G., Fetter, R.D., Shen, K., and Bargmann, C.I. (2008). GFP Reconstitution Across Synaptic Partners (GRASP) defines cell contacts and synapses in living nervous systems. Neuron 57, 353-363.

Iwanir, S., Tramm, N., Nagy, S., Wright, C., Ish, D., and Biron, D. (2013). The microarchitecture of C. elegans behavior during lethargus: homeostatic bout dynamics, a typical body posture, and regulation by a central neuron. Sleep 36, 385-395.

Kato, S., Kaplan, H.S., Schrodel, T., Skora, S., Lindsay, T.H., Yemini, E., Lockery, S., and Zimmer, M. (2015). Global brain dynamics embed the motor command sequence of Caenorhabditis elegans. Cell 163, 656-669.

McMiller, T.L., and Johnson, C.M. (2005). Molecular characterization of HLH-17, a C. elegans bHLH protein required for normal larval development. Gene 356, 1-10.

Mello, C., and Fire, A. (1995). DNA transformation. Methods Cell Biol. 48, 451-482.

Nath, R.D., Chow, E.S., Wang, H., Schwarz, E.M., and Sternberg, P.W. (2016). C. elegans Stress-Induced Sleep Emerges from the Collective Action of Multiple Neuropeptides. Curr. Biol. 26, 2446-2455.

Popovici, C., Isnardon, D., Birnbaum, D., and Roubin, R. (2002). Caenorhabditis elegans receptors related to mammalian vascular endothelial growth factor receptors are expressed in neural cells. Neurosci. Lett. 329, 116-120.

Press, W.H., Teukolsky, S.A., Vetterling, W.T., Flannery, B.P. (2007). Numerical Recipes: The Art of Scientific Computing, 3rd ed (New York, NY, USA: Cambridge University Press).

Welch, L.R. (2003). Hidden Markov models and the Baum-Welch algorithm. IEEE Information Theory Society Newsletter 53.

Yandell, M.D., Edgar, L.G., and Wood, W.B. (1994). Trimethylpsoralen induces small deletion mutations in Caenorhabditis elegans. Proc. Natl. Acad. Sci. USA 91, 1381-1385.